Chapter 15

Stereoelectronic Effects: Analysis by Computational and Theoretical Methods

Gabriel dos Passos Gomes and Igor Alabugin

Department of Chemistry and Biochemistry
Florida State University, USA

15.1 Introduction

One of the important roles of computational techniques in organic chemistry is in translating "fuzzy" qualitative concepts developed for rationalizing the vast diversity of empirical observations into the rigorous and quantitative language of quantum chemistry. The goal of this chapter is to illustrate the utility of computational methods for quantitative analysis of stereoelectronic effects.

"Stereoelectronic" is occasionally confused with "steric + electronic"! This is inaccurate. Stereoelectronic effects are stabilizing interactions originating from increased delocalization in a favorable conformation.[1] Repulsive steric interactions also depend on the spatial arrangement of orbitals but have a different electronic origin and, generally, are not considered as a part of stereoelectronic effects family.

More rigorously, stereoelectronic effects are defined as stabilizing electronic interactions maximized by a particular geometric arrangement which can be traced to a favorable orbital overlap. These

effects are ubiquitous in chemistry, and such orbital interactions can stabilize required conformations and reactive intermediates, deliver electron density to electron-deficient centers, synchronize bond forming and bond breaking, differentiate between alternative transition states (TSs), etc. Furthermore, such interactions can involve orbitals from different molecules or from different parts of the same molecule (i.e., be either inter- or intramolecular). Often, different layers of stereoelectronic interactions co-exist and co-evolve by coming into play at different stages of a multistep transformation.

The difficulty in applying the concept of stereoelectronic effects is associated with the flip side of its generality. Broad variations exist in the properties of donor and acceptor orbitals that can be stereoelectronically coupled. It is hard to have confidence with the relative donor ability of C–H and C–C bonds, especially if hybridization of carbon atoms in these bonds are different — such discussions have been heated and controversial.[2] Again, hybridization in particular can have confusing consequences that counteract electronegativity. For example, intuition can be misleading when comparing a p-orbital at oxygen with a sp^5 orbital at nitrogen where electronegativity and hybridization effects are directed in opposite ways.

15.2 Types of overlap in two-orbital interactions

In the language of molecular orbital (MO) theory, the most common situation corresponds to a stabilizing two-electron interaction involving two orbitals: a filled bonding orbital and an empty antibonding orbital (Fig. 15.1).

For the intermolecular formation of a chemical or supramolecular bond between two interacting fragments, the co-linear overlap of interacting orbitals is preferred, leading to the textbook description of supramolecular stereoelectronic effects such as H-bond formation. This orbital interaction pattern resembles direct-overlap in a σ-bond (Fig. 15.2(a)).

For molecules where the interacting atoms are already connected via a σ-bond, the dominant orbital interaction pattern corresponds to the π-type overlap. For example, the π-overlap is important

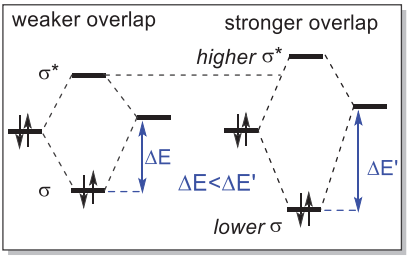

Figure 15.1. Formation of two-center two-electron chemical bonds and role of overlap in bond strength.

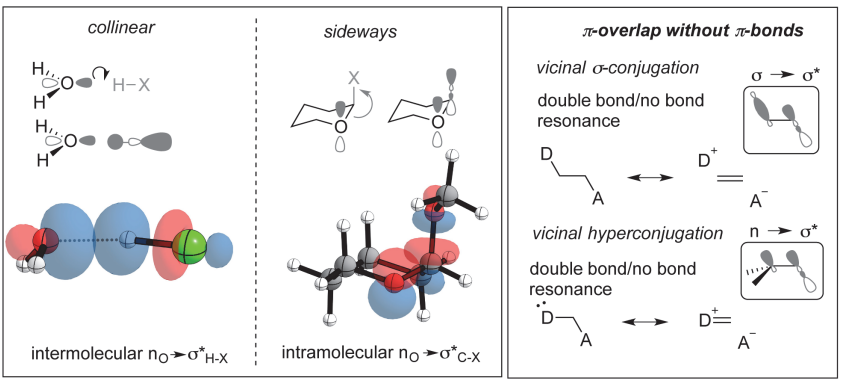

(a) (b)

Figure 15.2. (a) Comparison of intermolecular and intramolecular overlap patterns for interaction between lone pairs and antibonding orbitals. (b) Examples of interactions using π-overlap in systems lacking formal double bonds in the main Lewis structure.

in vicinal hyperconjugative interactions (Fig. 15.2(b)), providing stereoelectronic basis to such phenomena as the anomeric effect, gauche effect, and *cis*-effect (*vide infra*).

15.3 Computational and theoretical approaches for studies of stereoelectronic effects

Even though stereoelectronic effects manifest themselves in a variety of conformational preferences and reactivity effects,[1a] their precise experimental measurement can be challenging because structure,

properties, and reactivity can originate from a combination of multiple effects. Gauging the relative importance of coexisting effects can be greatly facilitated with the help of modern theoretical and computational advances. Section 15.3.1 will provide a general description of theoretical approaches to understanding, detecting, and quantifying stereoelectronic effects.

15.3.1 *Conformational changes*

The simplest and historically most important approach to quantifying stereoelectronic effects is based on conformational analysis (see Chapter 5). Conformational changes provide a convenient way to change orbital overlap responsible for the interaction in question. More importantly, conformational analysis unites experiment and theory because the quality of computed conformational profiles can be cross-checked with the experimental measurements. When experimental energies are used to benchmark computational methods, the appropriate choices can be made for the level of theory that can provide the right compromise between the accuracy and speed of calculations. High level conformational profiles also provide the necessary geometries for quantification of stereoelectronic effects with computational dissections described in the following sections on natural bond orbital (NBO) analysis and related methods.

The dependence of energies from rotation around single bonds is very general, as illustrated by the selection of examples provided in Fig. 15.3. The conformational preferences illustrated there involve a variety of functional groups with σ-bonds, π-bonds, and lone pairs that adopt well-defined geometries, very often with the antiperiplanar arrangement of the best donor and the best acceptor.[3]

However, the differences in conformer energies can potentially originate from multiple sources, leaving room for controversies and discussions regarding the relative importance of multiple components. Even when specific interactions can be "switched off" by a conformational change, more often than not, turning off one interaction activates another one.

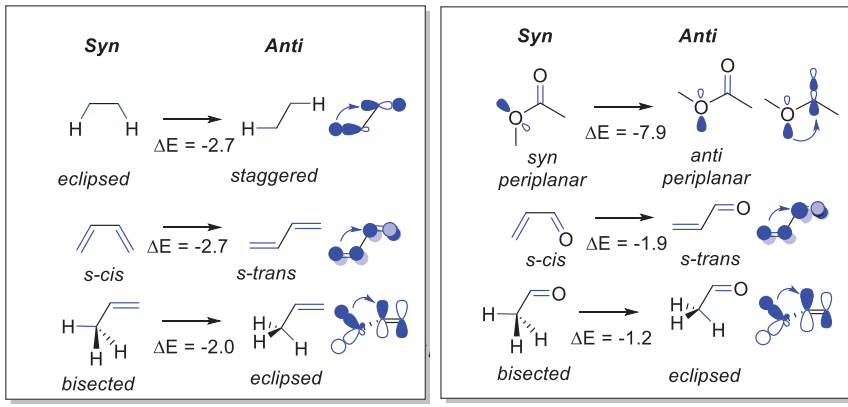

Figure 15.3. Energy differences for conformers originating from rotation around a single bond, from an anti to a syn arrangement between key interacting orbitals (shown in blue).

15.4 Isogyric, isodesmic, hypohomodesmotic, homodesmotic, and hyperhomodesmotic equations

In order to "isolate" a desired electronic effect, chemists often design hypothetical reactions of different degrees of sophistication (see Chapter 7). The advantage of these equations is that, in many cases, the thermochemical data can either be obtained experimentally or calculated with a high degree of accuracy. The challenge lies within zooming in on the key electronic effect without introducing additional structural and electronic perturbations. An "ideal" reaction for the analysis of a delocalizing electronic effect would involve no changes in hybridization and bond types. In addition, it should also have negligible changes in steric and electrostatic factors. Meeting all of these requirements is often a challenge.

The hierarchy of these equations was comprehensively summarized in a recent work by Wheeler *et al.*[4] We will discuss this order only briefly but will provide several examples to illustrate the possible caveats.

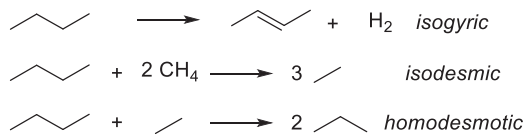

Figure 15.4. The simplest isogyric, isodesmic, and homodesmotic equations for butane.

Such equations can be divided into the categories: isogyric, isodesmic, and homodesmotic (further divided into hypohomodesmotic, homodesmotic, or hyperhomodesmotic). The level of accuracy and sophistication increases in the following order, where each next category is a subclass of the previous one: isogyric (RC1) $\supseteq$ isodesmic (RC2) $\supseteq$ hypohomodesmotic (RC3) $\supseteq$ homodesmotic (RC4) $\supseteq$ hyperhomodesmotic (RC5).

An illustration of the differences between simple isogyric, isodesmic, and homodesmotic equations is given in Fig. 15.4. The detailed definitions are given below.

15.4.1 *Isogyric equations*

This is the least restrictive comparison. In isogyric reactions (RC1), the total number of electron pairs is conserved but the number of specific bonds of a given type does not need to be balanced. Many reactions used in undergraduate chemistry textbooks (e.g., hydrogenation reactions) are isogyric.

15.4.2 *Isodesmic equations*

For hydrocarbons, the subset of isogyric reactions in which the number of C–C bonds of a given formal type (single, double, and triple) is conserved was defined as isodesmic (from Greek, *desmos* = bond) by Pople *et al.* in 1970.[5] Isodesmic reactions (RC2) are defined by preserving the number of bonds of each formal type (i.e., the single, double, or triple C–C bonds) in both reactants and products, and they include "bond separation reactions," a term for equations in which each bond between nonhydrogen atoms is separated into

the simplest two-heavy-atom fragments with the same formal bond types.

- Difference from isogyric equations: Formal type of bonds (single, double, triple, etc.) is conserved.

15.4.3 *Homodesmotic equations*

Homodesmotic ("equal bonds") equations are separated further into hypohomodesmotic (RC3), homodesmotic (RC4), and hyperhomodesmotic equations (RC4).

15.4.4 *Hypohomodesmotic reactions (RC3)*

(1) Equal numbers of carbon atoms in their various states of hybridization in reactants and products;
(2) Equal number of carbon atoms (regardless of hybridization state) with zero, one, two, and three hydrogens attached in reactants and products (i.e., CH, CH_2, CH_3 groups).

- Difference from isodesmic equations: The types of bonds are preserved, including heavy-atom hydrogen bonds. Carbon hybridizations are conserved.

15.4.5 *Homodesmotic reactions (RC4)*

(1) Equal numbers of carbon–carbon [Csp^3–Csp^3, Csp^3–Csp^2, Csp^3–Csp, Csp^2–Csp^2, Csp^2–Csp, Csp–Csp, Csp^2=Csp^2, Csp^2=Csp, Csp=Csp, Csp≡Csp] bond types in reactants and products;
(2) Equal number of each type of carbon atom (sp^3, sp^2, sp) with zero, one, two, and three hydrogens attached in reactants and products.

- Difference from hypohomodesmotic equations: The hybridization of partners in the individual C–C and C–H bonds is preserved.

15.4.6 *Hyperhomodesmotic reactions (RC5)*

(1) Equal number of carbon–carbon [H_3C–CH_2, H_3C–CH, H_2C–CH_2, H_3C–C, H_2C–CH, H_2C–C, HC–CH, HC–C, C–C, H_2C=CH, HC=CH, H_2C=C, HC=C, C=C, HC≡C, and C≡C] bond types in reactants and products;
(2) Equal numbers of each type of carbon atom (sp^3, sp^2, sp) with zero, one, two, and three hydrogens attached in reactants and products.

- Difference from homodesmotic equations: Same number of C–H bonds at identically hybridized fragments.

15.5 Examples

An example of an instructive and accurate equation is provided by that for biradical stabilization energies for the estimation of electronic interaction between the two radical centers in *p*-benzynes.[6] Although the two radicals do not overlap in space, they couple the σ^* orbitals of the C–C bridges ("through-bond coupling"). This interaction not only renders the Bergman cyclization to be a symmetry-allowed process[7] but also has important consequences for the reactivity of these species. All radical reactions of *p*-benzynes (i.e., H-abstraction, addition, etc.) have to pay a penalty for uncoupling the electrons, i.e., losing the through-bond interaction (estimated as $\sim 2-5$ kcal/mol).[8] This interaction can be conveniently evaluated by the "radical separation" equation in Fig. 15.5. Note that all bond types and hybridizations are balanced perfectly in this hyperhomodesmotic equation.

Although accurate, homodesmotic equations are often avoided due to their seeming complexity. However, useful information can also be obtained when isodesmic or isogyric equations are combined. As an example, let us analyze equations designed to evaluate the stabilization provided to a carbonyl group by a cyclopropyl substituent.

Because bent C–C bonds of cyclopropanes are good hyperconjugative donors, they are expected to lead to significant

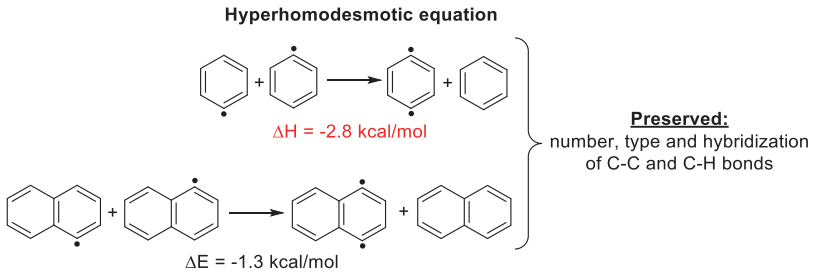

Figure 15.5. Appropriate hyperhomodesmotic equations display stabilization due to the through-bond coupling between the two radical centers of p-benzyne and its naphthyl derivative.

$\sigma_{C-C} \rightarrow \pi^*_{C=O}$ donation. This stabilizing effect accounts for the decreased reactivity of cyclopropyl esters in reactions where such donation is lost, like the formation of the tetrahedral intermediate of the acid- and base-promoted hydrolysis. Based on this hyperconjugative effect, cyclopropyl esters have been suggested as potential prodrugs with enhanced hydrolytic stability.[9] "Replacement energies" from the equations in Fig. 15.6 suggest that a cyclopropyl group provides ∼2 kcal/mol more stabilization to the carbonyl than a methyl.

Note that one can convert the above equations into a more accurate form by converting two isogyric equations into one in a way that can partially cancel the errors. For example, one can subtract the two equations as shown in Fig. 15.7.

The resulting equation is hypohomodesmotic (where the types of bonds are conserved, but hybridization partners in bonds can be different), and thus is better balanced than the parent equations. Furthermore, the new equation provides a direct evaluation of the phenomenon in question (i.e., the relative conjugative donor ability of cyclopropane vs. methyl).

15.6 The limitations of reaction equations: Caveat emptor

The importance of careful design of reaction equations aimed to evaluate a theoretical concept cannot be overstated. Otherwise, such

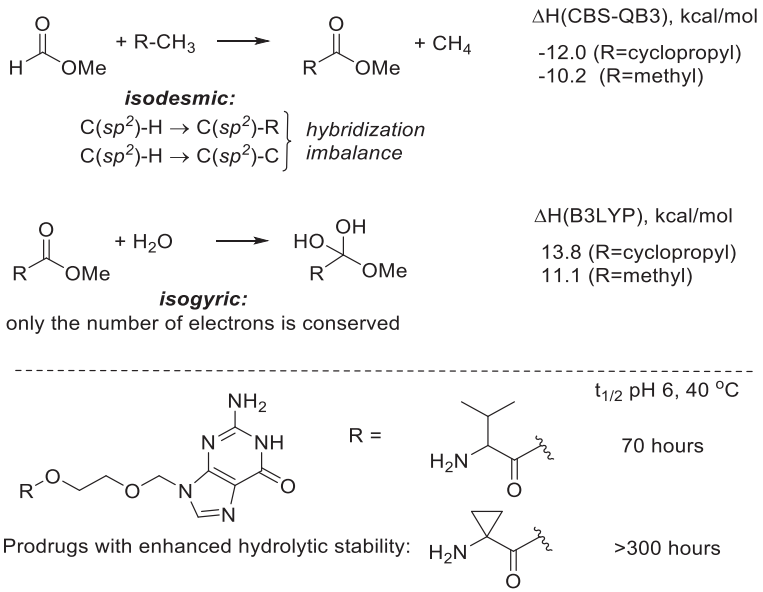

Figure 15.6. Control of the stability and reactivity of esters via $\sigma_{C-C} \rightarrow \pi^*_{C=O}$ interactions with strained cyclopropyl C–C bonds.

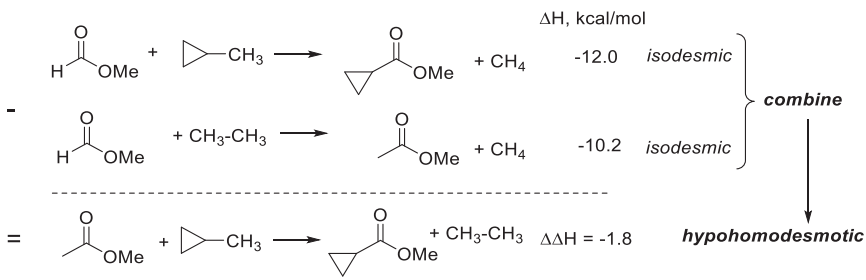

Figure 15.7. Converting a system of two isodesmic equations into a hypohomodesmotic equation by subtraction.

equations can lead to puzzling results such as the recent claim that "the conjugation stabilization of 1,3-butadiyne is zero".[10] Let us discuss this interesting example in detail.

The straightforward comparison of hydrogenation energies in two parent conjugated molecules, 1,3-butadiyne and 1,3-butadiene, revealed interesting differences (Fig. 15.8). Whereas the first

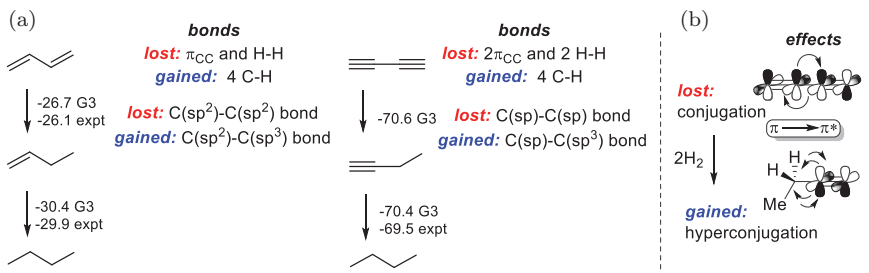

Figure 15.8. (a) Isogyric hydrogenation equations for butadiyne and butadiene. (b) Stereoelectronic origins of "disappearing" conjugative stabilization in butadiynes.

hydrogenation of a double bond in the diene is ∼3.8 kcal/mol less exergonic than the second hydrogenation, the complete hydrogenation of each of the triple bonds of butadiyne is equally exergonic. Because the difference between the two hydrogenation energies for the diene corresponds to the textbook example of conjugative stabilization, the absence of such difference in alkynes was suggested to indicate the lack of such conjugation in diynes. Clearly, this result is puzzling because one would expect resonance in conjugated diynes to be approximately twice of that in conjugated dienes. Why is it not so? Can the answer lie in the nature of equations used to describe this system?

It is immediately obvious that the hydrogenation equations are isogyric (not only are the bond types not conserved, but more importantly, the types of atoms are not conserved) and hence are not properly balanced. However, the lack of balance is not the main reason why these equations do not provide a physically reasonable estimate for the resonance stabilization of 1,3-diynes. This notion can be readily illustrated by converting the above equations into their more balanced version by subtracting equations for the first and second hydrogenation steps. Note that the resulting hypohomodesmotic equation conserves bond types but still provides the same surprising answer: "conjugation in butadiyne is close to zero!"

So, why does a better equation still not solve the problem? The real issue with the above equations is much larger. The key

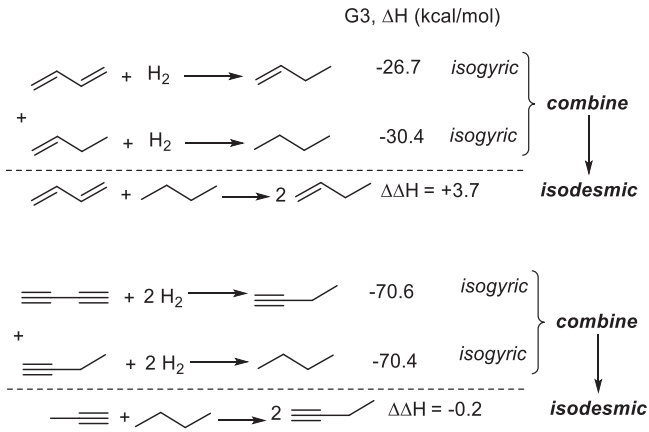

Figure 15.9. More balanced equations for butadiyne and butadiene still seem to suggest the "disappearance" of conjugative stabilization in butadiynes.

omission of Fig. 15.9 is its neglect of an important physical effect, i.e., hyperconjugation. The importance of hyperconjugation in alkynes is illustrated by the more appropriate isodesmic equations suggested by Jarowski *et al.*[11] For example, the difference between the heats of hydrogenation of ethylene and 1-butene provides an estimate for stabilization of ethylene (in kcal/mol) by an ethyl substituent (2.4 G3; 2.2 G3-(MP2); 2.7 experimental). Likewise, the hyperconjugative stabilization of acetylene by an ethyl group (4.9 G3; 4.8 G3-(MP2); 4.7 experimental) is evaluated by the difference between the heat of hydrogenation of acetylene and 1-butyne. Equivalently, the hyperconjugative stabilization can also be described by reactions in Fig. 15.9 that produce data consistent with the above evaluation.

Equations described in Fig. 15.10 illustrate that hyperconjugative stabilization of 1-butene and 1-butyne compensates for the loss of conjugative stabilization for butadiene only partially, but this compensation is complete in butadiyne. In other words, hyperconjugation in alkynes is twice as large as hyperconjugation in alkenes. This difference is sufficient for fully obscuring the conjugative stabilization in 1,3-butadiyne!

The take-home message here is the importance of designing meaningful, good-quality equations. Such equations must reflect the

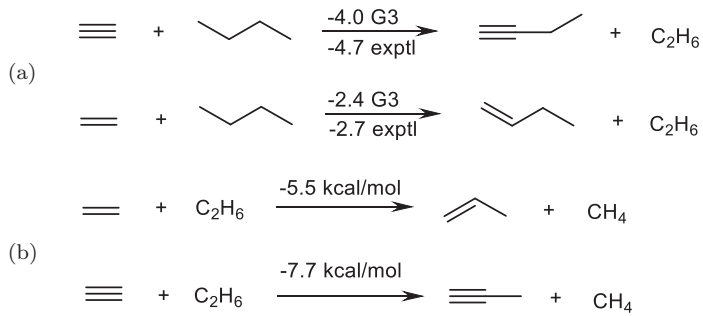

Figure 15.10. (a) Conventional equations for the evaluation of hyperconjugation. (b) Bond separation energy (BSE) values for alkene and alkyne hyperconjugation, corrected for protobranching.

Source: Reprinted with permission from Ref. [12].

answers raised by a particular problem. Not only should the types of bonds and atoms should be taken into account but specific physical phenomena (i.e., the interplay between different delocalization patterns) need to be properly balanced.

15.7 Dissecting electronic interactions

15.7.1 *Localized orbitals from delocalized wavefunctions*

The previous sections provided several indirect schemes for analyzing orbital interactions. One can see that isolating the desired effect is often difficult and sometimes impossible. Quantifying such electronic effects via a direct computational approach is seemingly straightforward. Conceptually, all one needs to do is calculate the energy penalty for removing this interaction from the delocalized wavefunction. The difference in energy between the noninteracting, localized state (sometimes called a diabatic state) and the full state (sometimes called adiabatic) can be taken then as the interaction energy. The main challenge lies in defining the appropriate localized state to serve as a reference point. Three approaches have emerged as popular tools for isolating delocalizing interactions (see Chapters 8 and 10): NBO analysis, Energy Decomposition

Analysis (EDA),[13] and the Block-Localized Wavefunction method (BLW).[14]

These methods share a conceptual similarity by starting with a hypothetical localized construct as the reference point. The key difference between these methods lies in the initial basis set of orbitals used. In contrast to NBO that starts with *orthogonal* orbitals to describe the localized reference, the other two methods use *nonorthogonal* orbitals to define the reference point.[15] This difference leads to significant variations in the estimated magnitude of delocalizing interactions. It also increases the apparent contribution from steric effects for the methods based on nonorthogonal orbitals.

The nonorthogonal initial orbitals cannot be the eigenfunctions of any physical (Hermitian) Hamiltonian corresponding to the reference "unperturbed system." Although the overlap contamination effects do not change energies evaluated on the basis of the *overall* molecular wavefunctions (whether orbitals of a determinate wavefunction are orthogonal or not has no effect on the overall expectation value), orbitals (and charge density) attributed to one group have overlap with (and thus could equally well be attributed to) orbitals of the other group. If the "bond" of one group overlaps with the "antibond" of the other group, such overlap will automatically be labeled "exchange repulsion" in a scheme based on nonorthogonal orbitals.[16]

The ambiguity about which nonorthogonal subunits receive credit for unaccounted density in the overlap region is the source of many reported differences between alternative computational dissections. The associated overlap density can be assigned to the filled orbital (and counted toward steric effects) or to the unfilled orbital (and counted toward hyperconjugative charge-transfer). All methods that harbor such overlap ambiguities are expected to differ sharply from NBO-based assessments of intramolecular or intermolecular interactions.

Furthermore, Fig. 15.11(a) illustrates the origin of "four-electron destabilization" between two nonorthogonal filled orbitals that is often taken as the physical origin of the steric destabilization.

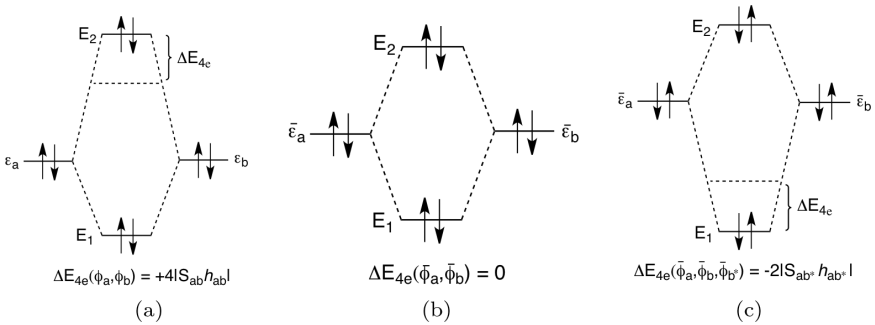

Figure 15.11. (a) Four-electron destabilizing interaction expressed in terms of nonorthogonal "unperturbed" orbitals (for which there is no imaginable Hermitian perturbation theory). (b) Four-electron nonstabilizing interaction expressed in terms of orthogonalized unperturbed orbitals (for which there exists a valid Hermitian). (c) Four-electron stabilizing interaction for a proper three-term description of orbital energies in terms of Löwdin-orthogonalized basis orbitals.

Source: Reprinted with permission from Ref. [17(b)].

According to Weinhold *et al.*, such destabilization is a mathematical artifact of nonorthogonality and does not, in fact, correspond to a physical interpretation of any imaginable physical process.[17] Once orbitals are orthogonalized, the "four-electron destabilization" disappears (Fig. 15.11(b)). When at least one unoccupied orbital is added to the system, the overall interaction becomes stabilizing (Fig. 15.11(c)).[17]

After this general preface, let us describe the three popular approaches in more detail.

15.7.2 *Natural bond orbital analysis*

The NBO analysis transforms the canonical delocalized Hartree–Fock (HF) MOs and nonorthogonal atomic orbitals (AOs) into the sets of localized "natural" atomic orbitals (NAOs), hybrid orbitals (NHOs), and bond orbital (NBOs). Each of these localized basis sets is complete, orthonormal, and describes the wavefunction with the minimal amount of filled orbitals in the most rapidly convergent fashion. Filled NBOs describe the hypothetical, strictly

localized Lewis structure. Natural Population Analysis (NPA) charge assignments based on NBO analysis correlate well with empirical charge measures.[18]

The interactions between filled and antibonding orbitals represent the deviation from the localized Lewis structure and can be used as a measure of delocalization. Since the occupancies of filled NBOs are highly condensed, the delocalizing interactions can be treated by a standard second-order perturbation approach (Eq. (15.1)) or by deletion of the corresponding off-diagonal elements of the Fock matrix in the NBO basis and recalculating the energy (referred to as E_{del} energies)[19,20] where $\langle\sigma|F|\sigma^*\rangle$, or F_{ij} is the Fock matrix element between the orbitals (NBOs) i and j, ε_σ and ε_{σ^*} are the energies of the σ and σ^* NBOs, and n_σ is the population of the donor σ-orbital.[21] Usually, there is a good linear correlation between the deletion (E_{del}) and perturbation ($E(2)$) energies.[22] Deviation from such correlation often reflects cooperativity between the individual delocalizing interactions.

$$E(2) = -n_\sigma \frac{\langle\sigma|F|\sigma^*\rangle^2}{\varepsilon_{\sigma^*} - \varepsilon_\sigma} = -n_\sigma \frac{F_{i,j^2}}{\Delta E} \tag{15.1}$$

Natural Steric Analysis[23] in the NBO procedure is based on the model of Weiskopf where orbital orthogonalization leads to the "kinetic energy pressure" that opposes interpenetration of matter.[24] As the orbitals begin to overlap, the physically required orthogonalization leads to additional oscillatory and nodal features in the orbital waveform, which correspond to increased wavefunction curvature and kinetic energy, the essential "destabilization" that opposes interpenetration. The overlap-type analysis of Pauli interactions can be introduced to the NBO framework through interactions of nonorthogonalized pre-NBOs.

The NBO procedure is not the only localization technique for transforming delocalized MOs into the intuitive Lewis structure description. Foster and Boys,[25] Edmiston and Ruedenberg,[26] and Pipek and Mezey[27] reported alternative localization procedures that

provide additional bridges between MO and valence bond (VB) theories.

From the organic chemist's point of view, these approaches are conceptually similar to NBO and, for the sake of brevity, will not be discussed herein.

The set of localized bonding Lewis systems can be extended to *3c-2e* bonds, and even to electron pairs localized over bigger fragments, via adaptive natural density partitioning (AdNDP).[28] When lone pairs are truly delocalized over all of the available atoms in a cyclic system, it can be taken as a sign of aromaticity (see Chapter 9).

15.7.3 *Energy decomposition analysis*[29]

This analysis starts with a "zeroth-order" wavefunction from the overlapping orbitals of the isolated molecular fragments (see Chapter 7). In EDA, the interactions between these fragments are divided into three steps. In the first step, the fragments, which are calculated with the frozen geometry of the entire molecule, are superimposed without electronic relaxation; this yields the quasi-classical electrostatic attraction ΔE_{elstat}. In the second step, the product wavefunction becomes antisymmetrized and renormalized, which gives the repulsive term ΔE_{Pauli}, termed Pauli repulsion. In the third step, the MOs relax to their final form to yield the stabilizing orbital interaction ΔE_{orb}. The latter term can be divided into contributions of orbitals having different symmetry which is useful for separation of σ- and π-effects. The sum of the three terms $\Delta E_{\text{elstat}} + \Delta E_{\text{Pauli}} + \Delta E_{\text{orb}}$ gives the total interaction energy ΔE_{int}.

The utility of EDA is illustrated by comparison of conjugation and hyperconjugation by Fernandez and Frenking,[30] who suggested that hyperconjugation is roughly half as strong as π-conjugation between two multiple bonds and that the hyperconjugative stabilization of C–H and C–C bonds with double bonds is half as strong as such stabilization by the triple bonds. As a result, hyperconjugative stabilization of the two π-systems in alkyl substituted alkynes (20.1 kcal/mol) such as 1-propyne and 4,4-dimethyl-1-butyne

is almost identical as the conjugative stabilization in 1,3-butadiene (19.5 kcal/mol).

15.7.4 *Block localized wavefunction method*[31]

The electron delocalization to the cationic carbon and neutral boron center can be estimated by removing the vacant *p*-orbitals from the expansion space of MOs. Although this simple orbital deletion procedure (ODP) technique is limited to the analysis of positive hyperconjugation in carbocations and boranes, it has been generalized and extended to the BLW method.[32–34]

The BLW method combines the MO and VB theories. In this method, the wavefunction for a localized (diabatic) state is defined by limiting the expansion of each MO (called block-localized MO) to a predefined subspace. Block-localized MOs belonging to different subspaces are generally nonorthogonal. A conceptual advantage of this method is that the BLWs for diabatic states are optimized self-consistently, and the adiabatic state is a combination of a few (usually two or three) diabatic state wavefunctions.

For example, for propene, the delocalized and localized (BLW) wavefunctions can be expressed as $\Psi(\text{del}) = \hat{A}(\sigma 1a"^2 2a"^2)$ and $\Psi(\text{loc}) = \hat{A}(\sigma\pi^2_{c=c}\pi^2_{CH3})$, where $\pi_{C=C}$ and π_{CH3} are group orbitals expanded in CH_2=CH and CH_3 groups, and are nonorthogonal. In contrast, canonical MOs 1a" and 2a" are delocalized for the whole system and orthogonal. In this example, the energy difference between these two wavefunctions, which are independently optimized self-consistently, is taken as the vicinal hyperconjugative interaction between the π-double bond and the adjacent methyl group.

15.7.5 *Other approaches to wavefunction analysis*

The electronic structure and chemical bonding of molecular systems can also be described via Electron Sharing Indexes (ESI)[34] and other approaches that evaluate electronic sharing between two atoms using the concept of bond order (bond index).[35]

Alternatively, a variety of approaches to the analysis of chemical bonding avoids the notion of "chemical bonds" altogether and

replaces them with the analysis of charge density, such as the topological properties of the Laplacian of the electron density (quantum theory of atoms in molecules QTAIM),[36] or electron localization function (ELF) that defines "localization attractors" of bonding, nonbonding, and core type.[37]

In this part, we will provide several examples of practical evaluation of different types of delocalization. We will use NBO analysis for this purpose due to its close connection to classic concepts of chemical bonding.

15.8 Illustrative examples of NBO analysis of stereoelectronic interactions

15.8.1 *Types of delocalization: Neutral, negative, positive*

Hyperconjugation is the most common of the stereoelectronic effects. It can manifest itself in a number of physical observables such as bond lengths, bond angles, and quantifiable parameters such as orbital population, charges and orbital interaction energies. Let us start in a simple way and analyze three parent $H_3C–X$ systems of different electronic nature ($X = NH_2$, CH_3, BH_2) to calibrate our perception of negative, neutral, and positive hyperconjugation (see Fig. 15.12).

$MeNH_2$: Methyl amine presents a negative hyperconjugative $n_N \rightarrow \sigma^*_{CH}$ interaction, estimated by NBO analysis as worth 8.6 kcal/mol. This interaction has structural consequences as well. In particular, it elongates the adjacent C–H bond relative to the same C–H bond in ethane, and, at the same time, it shortens the C–N bond. These geometric changes are consistent with the "no-bond/double-bond" resonance structure that describes this delocalization. The geometric consequences of such interactions can be more accurately evaluated with optimization with such interactions "switched off" using NBO deletion procedures.

NBO analysis also allows one to analyze effects on orbital populations. For example, donation of electronic density from the N's lone pair to a vacant σ^*_{CH} orbital decreases the population of the former

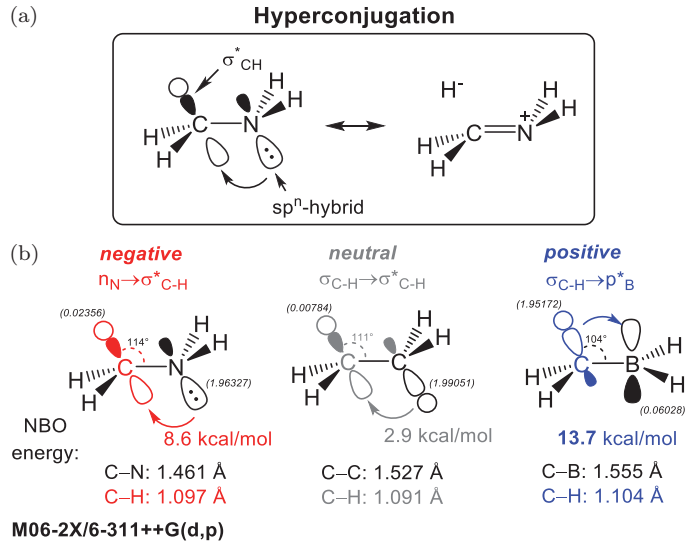

Figure 15.12. (a) General (negative) hyperconjugation with the "double bond/no bond" resonance of methylamine. (b) Examples of negative, neutral, and positive hyperconjugation. Note that neutral hyperconjugation needs to be multiplied by two since it is bidirectional.

(from 2 to 1.963 e, or, in other words, 0.037 e is missing from the lone pair) and increases population of the latter (from 0 to 0.023 e). The stereoelectronic connection between these effects is illustrated by the similarity of the two values and by the significantly greater populations of the "misaligned" vicinal C–H bonds (1.991 e).

$MeBH_2$: Delocalization in methylborane is dominated by positive hyperconjugation with a large $\sigma_{CH} \rightarrow p_B^*$ interaction (13.7 kcal/mol). The resonance description of such interaction as "double bond/no bond" is consistent with the elongation of the interacting C–H bond. The decrease of the H–C–B angle (when compared to H–C–H and even H–C–N angles) is associated with rehybridization of the donor C–H bond, which acquires much more *p*-character (79.91%) in comparison with the other two C–H bonds (76.51%). By aligning the C–H bond better with the boron's empty p-orbital, the molecule maximizes the donor–acceptor hyperconjugative interaction, thus gaining a greater stabilization.

Ethane: The neutral hyperconjugation observed in ethane is perfectly bidirectional, meaning that all antiperiplanar C–H bonds interact with each other both as a donor and an acceptor. By symmetry, these interactions are identical in magnitude. This situation is conceptually different from negative hyperconjugation, where a lone pair can only act as a donor, and from positive hyperconjugation, where an empty orbital can only act as an acceptor. However, neutral hyperconjugation can be rather imbalanced when different sets of donors and acceptors interact.

15.8.2 *Evolution of neutral hyperconjugation in polar molecules*

As an illustration of polar effects in hyperconjugation, let us compare fluoroethane, ethyllithium, and ethane (Fig. 15.13). The $\sigma_{CH} \rightarrow \sigma^*_{CH}$ interaction in ethane is estimated by NBO as worth 2.9 kcal/mol and, as it mentioned earlier, it is perfectly balanced by an identical interaction in the opposite direction. There is no net charge transfer between the two parts of the molecule. In ethyllithium, the situation is different. The $\sigma_{CLi} \rightarrow \sigma^*_{CH}$ donation is much stronger than the $\sigma_{CH} \rightarrow \sigma^*_{CLi}$ interaction (8.5 vs. 1.8 kcal/mol, respectively), so the C–Li bond is the net hyperconjugative donor in the C–H/C–Li pair. As expected, the balance in the C–F/C–H tug-of-war for electron density is shifted toward the C–F bond ($\sigma_{CH} \rightarrow \sigma^*_{CF} > \sigma_{CF} \rightarrow \sigma^*_{CH}$, 5.1 vs. 1.0 kcal/mol, respectively). Electronic density in the C–H bond antiperiplanar to the σ^*_{CF} (1.982 e) is depleted relative to the C–H bonds of ethane (1.990 e) and the *gauche* C–H bonds of fluoroethane (1.988 e).

Although the above trends are, of course, not surprising, the value of NBO dissection comes from the additional information that it provides. First, it gives an estimate of how large the differences in energies are. Second, NBO gives useful insight into the two factors that are responsible for the magnitude of orbital interactions for a pair of the donor and the acceptor orbitals, i.e., the contributions from the energy gap and the Fock matrix element (proportional to the orbital overlap). In this particular comparison of

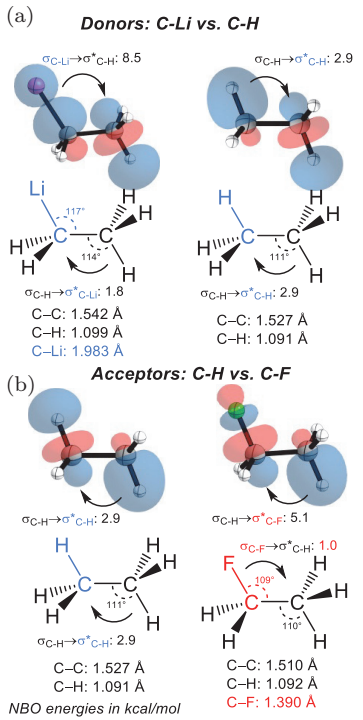

(c)

	orbital	Energy (a.u.)	Occupancy (electrons)
Li	$\sigma_{C\text{-}H}$	-0.51026	1.99250
	$\sigma_{C\text{-}Li}$	-0.26622	1.96399
	$\sigma^*_{C\text{-}H}$	+0.52019	0.02557
	$\sigma^*_{C\text{-}Li}$	+0.18888	0.00408
H	$\sigma_{C\text{-}H}$	-0.55974	1.99051
	$\sigma^*_{C\text{-}H}$	+0.48440	0.00784
F	$\sigma_{C\text{-}H}$	-0.58286	1.98269
	$\sigma_{C\text{-}F}$	-1.03228	1.99707
	n_F	-0.48800	1.97484
	$\sigma^*_{C\text{-}H}$	+0.46421	0.00451
	$\sigma^*_{C\text{-}F}$	+0.30841	0.02158

Figure 15.13. (a) Comparison of donor ability between C–Li and C–H bonds. (b) Comparison of acceptor ability between C–H and C–F bonds. (c) Energy and population of the orbitals in ethyllitium, ethane, and fluoroethane.

the three substituted "ethanes," the NBO dissection clearly show that the difference in the energies of delocalizing interactions comes from both sources, but the relative contributions are different. From the second-order perturbation energy equation, it is clear that the Fock matrix element $F_{i,j}$ contribution is dominant, especially in ethyllithium (Fig. 15.14).

In addition to evaluating individual orbital contributions, NBO can also evaluate the "global" importance of resonance for the whole molecule. This can be done by comparing the total amount of "non-Lewis density" in the NBO output. Interestingly, this parameter shows that, overall, ethyllithium is slightly less delocalized than ethyl fluoride ("valence non-Lewis density" for EtLi is 0.367% vs. 0.381%

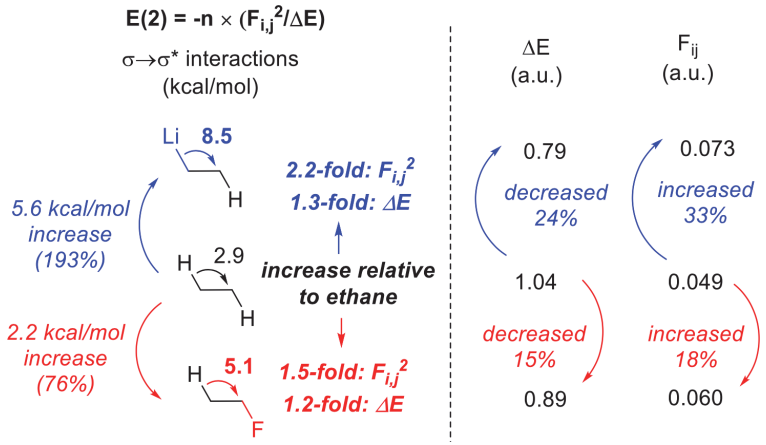

Figure 15.14. Analysis of $F_{i,j}$ and ΔE terms in the hyperconjugative interactions. The second-order perturbation energy equation illustrates that the $F_{i,j}$ term is the dominant component in the σ-conjugation strengthening observed for more polar bonds.

for EtF). This finding may look surprising considering the great magnitude of the σC−Li → σ^*C−H interaction discussed above. However, one should not forget the presence of multiple lone pairs at the fluorine atom. These lone pairs are strongly delocalized through negative hyperconjugation interactions (nF → σ^*C−H and nF → σ^*C−C) that are not present in EtLi.

15.8.3 *Overlap effects on hyperconjugative interactions in the absence of polarization*

When analyzing the concentration of interactions between bonds of different polarity, one should not forget that simple geometric factors have a large effect on the magnitude of delocalizing interactions. For example, even the neutral C–H/C–H hyperconjugation can be increased by ∼80% in magnitude when the interacting orbitals are separated by the shorter C=C bond of ethene. It is noteworthy that this large change is a consequence of just a 0.2 Å decrease in the distance between two carbon atoms.

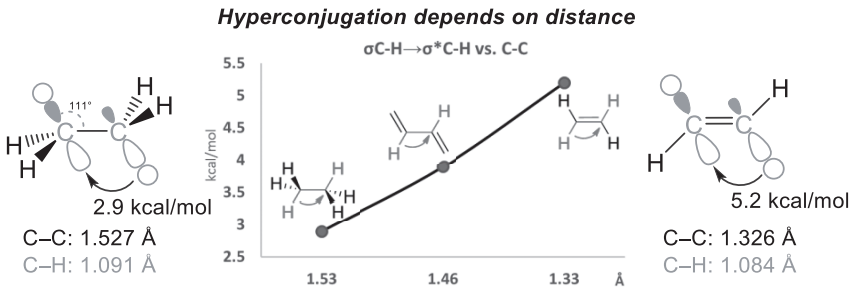

Figure 15.15. The dependence of hyperconjugation from the distance between two interacting orbitals in representative hydrocarbons.

The dominating role of C–C distance, rather than hybridization, is further illustrated by the comparison of such interaction in 1,3-butadiene where the antiperiplanar C–H bonds at the central atom are separated by a C(sp^2)–C(sp^2) bond. Although the C–C bond-forming hybrids have the same hybridization as in the C–C bond of ethane, there is only partial double bond order and the C–C distance is longer. As a result, the $\sigma_{C-H} \rightarrow \sigma^*_{C-H}$ interaction energy lies between that in ethane and ethene (Fig. 15.15).

15.8.4 *Directionality of stereoelectronic effects*

The above examples provided quantitative insights but for the systems that are relatively simple and intuitively understandable. In the present section, we will provide analysis of less obvious, yet important, effects associated with directionality of stereoelectronic interactions. In order to illustrate this phenomenon, let us compare two similar interactions in ethyl methyl ether: $\sigma_{CH} \rightarrow \sigma^*_{C-O}$ and $\sigma_{CH} \rightarrow \sigma^*_{O-C}$. The interactions involve the same σ^* acceptor that overlaps, at its opposite ends, with two analogous σ_{C-H} donors. Despite these similarities, the magnitude of these effects is noticeably different: acceptor ability of the bridge bond increased by 38% (from 3.2 to 4.4 kcal/mol) at the carbon end relative to the oxygen end (Fig. 15.16).

NBO analysis readily answers why C–O bonds are ∼40% better acceptors than O–C bonds in $\sigma_{C-H} \rightarrow \sigma^*_{X-Y}$ interactions

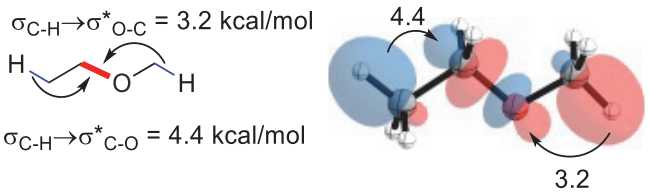

Figure 15.16. Polarization of C–O bond dramatically changes the magnitude of interactions depending on the C or O end of its antibonding orbital.

(X, Y=O, C) in ethers. The origin of this directionality lies in polarization of σ^*_{CO} orbital.[24] Due to the greater electronegativity of carbon, the carbon end of the σ^*_{CO} orbital has the larger orbital coefficient, leading to a larger $F_{i,j}$ term for the $\sigma_{C-H} \rightarrow \sigma^*_{C-O}$ interaction.

However, the expectations based on electronegativity fail to provide an explanation for an even stronger directionality of hyperconjugative interactions in the analogous sulfur compounds. This observation is not consistent with bond polarization. Not only is the difference in electronegativity between carbon and sulfur considerably smaller than between carbon and oxygen, but a C–S bond is polarized toward C and therefore its antibonding orbital has a greater orbital coefficient at S.

So what is the origin of this surprising behavior? Figure 15.17 illustrates that the 1,3-dithiane ring is distorted because S–C bonds are longer than C–C bonds. This geometric feature imposes very different orbital overlaps,[38] leading to a larger difference in magnitude between $\sigma_{C-H} \rightarrow \sigma^*_{C-S}$ (5.6 kcal/mol) vs. $\sigma_{C-H} \rightarrow \sigma^*_{S-C}$ (1.3 kcal/mol).

Directionality and anisotropy of stereoelectronic effects manifests itself often in more complex systems, especially when stronger donors such as lone pairs are present. Recently, such effects were shown to contribute to the structural and electronic differences between peroxides and ethers (and between acetals and bis-peroxides).[39]

In these systems, the directionality of $n_O \rightarrow \sigma^*_{X-Y}$ interactions is pronounced even further. At the same level of theory, the NBO energy for $n_O \rightarrow \sigma^*_{C-O}$ interaction in the acetal is worth 14.9 kcal/mol,

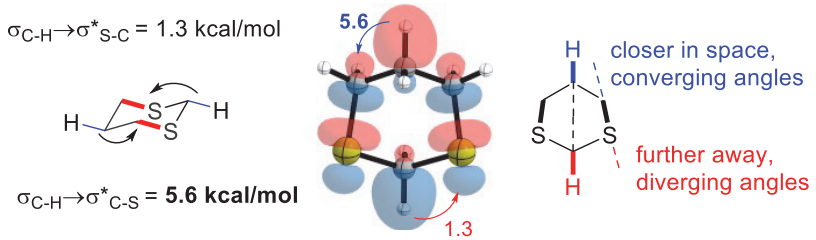

Figure 15.17. The difference in energy of the hyperconjugative interactions in 1,3-dithiane stem from different orbital overlaps rather than (lack of thereof) polarization of the C–S bond.

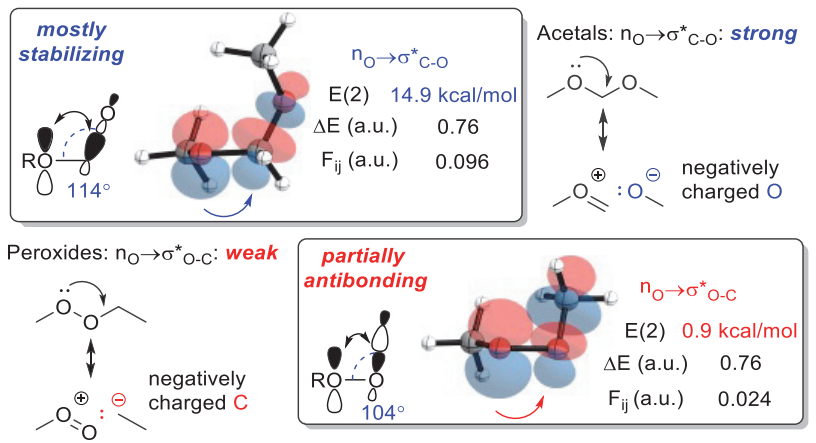

Figure 15.18. The difference between $n_O \rightarrow \sigma^*_{C-O}$ interactions in acetals and $n_O \rightarrow \sigma^*_{O-C}$ interactions in peroxides is amplified by more than 16-fold (>1600% difference!).

whereas the energy $n_O \rightarrow \sigma^*_{O-C}$ interaction in the peroxide is worth ~0.9 kcal/mol (Fig. 15.18). In other words, the stereoelectronic difference increased from 40% to more than 1600% in the σ^* interactions with a stronger donor (σ_{C-H} vs. n_O, see Fig. 15.17 vs. 15.18).

The reason for the greatly increased hyperconjugative anisotropy lies in the intricate combination of effects that control the resulting orbital overlap. When a σ-orbital serves as a donor, most of the stabilizing orbital overlap in the $\sigma \rightarrow \sigma^*$ interaction originates from overlap of this σ-orbital with the *back* lobe of an antiperiplanar

σ^*-acceptor. In contrast, when a p-orbital serves as a donor in an anomeric interaction, the notions of syn- and antiperiplanarity vanish. In such systems, the n_p/σ^* overlap is significant with both the back lobe of the σ^* orbital (e.g., from the O–C bond in the peroxide in Fig. 15.18) and the antibonding region between the two atoms (e.g., O and C). In peroxides, the unusually small O–O–C angle brings the σ^*_{OC} node closer to the p-orbital. The destabilizing interaction with the out-of-phase hybrid at carbon largely offsets the in-phase stabilizing interaction of the p-donor with the oxygen part of the σ^*_{O-C} orbital (Fig. 15.18).

The greater than 16-fold decrease in the magnitude of $n_O \rightarrow \sigma^*_{\mathbf{O-C}}$ interactions in peroxides in comparison to $n_O \rightarrow \sigma^*_{\mathbf{C-O}}$ interactions in acetals is striking. Taken together with the above-mentioned structural effects, the nonsymmetric nature of σ-acceptors explains why the anomeric effect is dramatically diminished in peroxides in comparison with acetals. This stereoelectronic analysis reveals the weakening of anomeric hyperconjugative interactions as an additional source of thermodynamic instability of dialkyl peroxides.

A logical expansion of this stereoelectronic analysis explains why bis-peroxides can possess surprising stability. When the second peroxide moiety in the same molecule is separated by from the first peroxide by a one-atom bridge, such bis-peroxides can be considered as acetals. In cyclic molecules of this family, the two peroxide moieties stabilize each other via strong anomeric $n_O \rightarrow \sigma^*_{\mathbf{C-O}}$ interactions (Fig. 15.19). Note that the NBO dissection and isogyric and isodesmic equations agree in identifying the increased stability of bis-peroxides.

15.8.5 *Multilayered orbital interactions in carbonyl compounds*

In this section, we show how NBO analysis can be used for the dissection of hyperconjugative interactions in organic functional groups using ketones as a molecular guinea pig. A pedagogically interesting feature of this important class of organic molecules is that

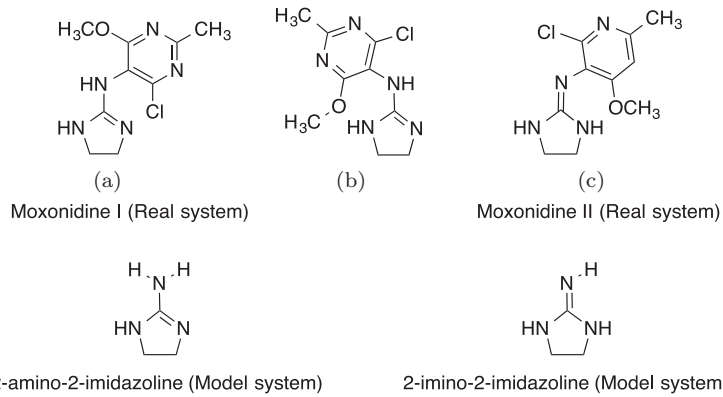

Figure 15.19. Relative weakness of hyperconjugative donation from oxygen lone pairs to vicinal σ^*-acceptors in peroxides vs. acetals (top) and stereoelectronic transformation of bis-peroxides to bis-acetals (bottom).

they contain all major types of orbitals: σ-bonds, π-bonds, and lone pairs. Let us discuss the key orbital interactions revealed by NBO analysis.

The "first level" of interactions involve delocalization of C–H bonds with $\pi_{C=O}$. Note that this interaction increases when C–H bonds are anti to a carbonyl π-bond (i.e., in the eclipsed conformation). The respective combined NBO energies for the π-component of donation to and from the carbonyl increase from 13.2 vs. 14.9 kcal/mol. One could stop here, because this answer does capture the most important change in the magnitude of delocalization. Furthermore, the greater stabilizing effect is observed in the more stable (eclipsed) conformation (*vide infra*). However, it is instructive to take a moment and examine the vicinal effects in greater detail, getting a closer view of the full complexity of this system, which originates form the interplay between multiple delocalizing interactions of different nature (Fig. 15.20).[40]

The "second level" of interactions that are also different in the bisected and eclipsed conformations of ethanal includes the vicinal interactions between anti- and syn-periplanar σ-bonds. Note that changes in the individual interactions are substantial. For example, the 0.9 kcal/mol interaction of the in-plane C–H bond with

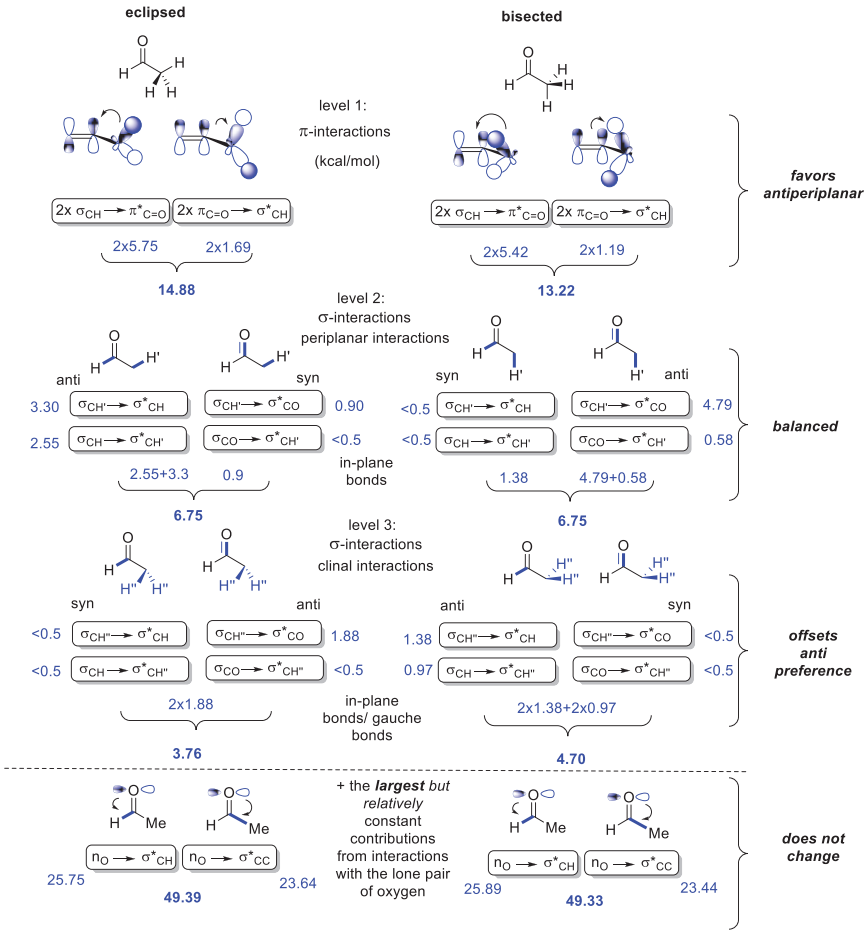

Figure 15.20. NBO analysis of stereoelectronic interactions involved in the conformational profile of ethanal. The combined energies should be treated as approximate because interaction with energies below the default NBO threshold of 0.5 kcal/mol was not used in determining the overall balance.

the σ^*_{C-O} orbital increases to 4.8 kcal/mol due to the change from syn- to anti-periplanar orbital arrangement. Note that the change in energy of $\sigma_{C-H} \rightarrow \sigma^*_{C-H}$ interactions between the two vicinal in-plane C–H bonds partially compensates for the difference in C–H/π_{C-O} interactions.

The "third level" of resonance delocalization involves the imperfectly aligned syn- and anticlinal vicinal σ-bonds. Here, the effect of $\sigma_{C-H} \rightarrow \sigma^*_{C-H}$ interactions favors the bisected conformation where these orbitals are anticlinal. However, this effect is smaller and cannot overcome the π-effects that impose a greater bias toward the eclipsed conformation.

Interestingly, the strongest hyperconjugative effect in this system, the $n_O \rightarrow \sigma^*$ delocalization, remains a bystander that it is fully impartial to the "eclipsed vs. bisected" conformational tug-of-war. Although the $n_O \rightarrow \sigma^*$ interactions are very large (23–26 kcal/mol), they change only slightly upon conformational change. They are important for determining the overall stability of carbonyl compounds but impose hardly any effect on the conformational equilibrium.

There are several take-home messages from this analysis. First, the several layers of conjugative interactions illustrate the electronic richness that can hide even in a relatively simply system. A subset of these interactions can play a determining role in a specific conformational or reactivity feature whereas the other factors may play a secondary role that can be either cooperative or anticooperative. Figure 15.20 illustrates how the qualitative analysis based on the quantum-mechanical dissection of the high-quality wavefunctions (such as NBO analysis) can help to untangle this complexity. Furthermore, the balance between different "levels" of interactions can change upon physical or chemical changes in the environment.

Let us now summarize conformational profiles of carbonyl compounds and show how the interplay between the first three layers of hyperconjugation in Fig. 15.20 can explain the relative stabilities of aldehyde conformations. The eclipsed conformation is favored over the bisected in straight chain aldehydes and ketones.[41] Contrary to the expectations based on steric reasoning, linear alkyl groups prefer to eclipse the carbonyl. For example, the doubly methyl-eclipsed conformation is the most stable rotamer of 3-pentanone. For the larger alkyl groups (i.e., *t*-butyl), the preference is for the hydrogen group to

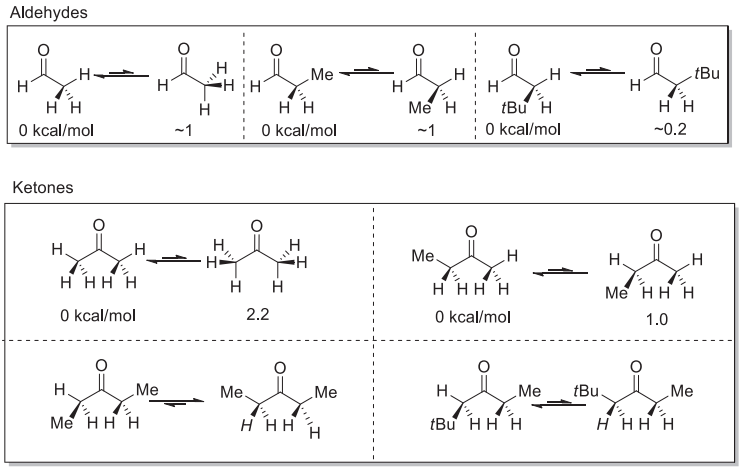

Figure 15.21. Stereoelectronic preference for the eclipsed conformation in carbonyl compounds, analogous to the preference in alkenes.

eclipse the carbonyl (Fig. 15.21). These conformational preferences are general. For example, similar trends, not conforming to a model based on sterics, are observed for alkenes.[42] This conformational effect can be traced back to the slightly higher donor ability of σ_{CH} bonds over that of σ_{CC} bonds in $\sigma \rightarrow \pi^*$ interactions. Delocalization in carbonyls is less balanced and more unidirectional than it is in alkenes: the $\sigma_{CH} \rightarrow \pi^*_{C=O}$ interactions become more important in carbonyls, as the $\pi^*_{C=O}$ acts as a better acceptor due to polarization and the higher electronegativity of oxygen.

It is important to mention that effects that are invisible and "unimportant" for conformational equilibria (e.g., the "fourth level" of delocalization in Fig. 15.20) can play key roles in reactivity. For example, the large $n_O \rightarrow \sigma^*_{C-H}$ interaction in aldehydes evolves, upon the C–H bond scission, into a $2c{-}3e$ bond in acyl radical. The latter effect manifests itself as the source of dramatic weakening of the aldehyde C–H bond dissociation energy (BDE) (∼88 kcal/mol) — much smaller than the BDE for a C–H bond in ethane (∼111 kcal/mol; Fig. 15.22).[43] The difference is especially striking, since both carbon atoms are sp^2 hybridized and expected to have relatively strong

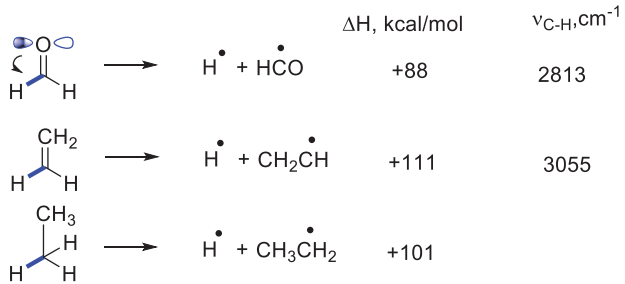

Figure 15.22. The large $n_O \rightarrow \sigma^*_{C-H}$ interactions manifest themselves as decreased C–H bond BDE and red-shifted C–H stretching frequencies in aldehydes.

C–H bonds. However, the C(O)–H bond in aldehydes is even weaker than a typical C–H bond in alkanes. This structural feature and the resulting ease of acyl radical formation has important consequences for the stability and reactivity of aldehydes under radical-forming conditions.

15.8.6 *Competition between hyperconjugation and (re)hybridization/polarization*

Stereoelectronic effects compete with other factors, such as direct changes in bond polarization and hybridization. Although the interplay between conjugation and hybridization/polarization effects can be complex, methods such as NBO analysis allow one to evaluate the relative variations in such effects, identifying the regions where either hybridization or hyperconjugation can dominate. Such analysis can be very helpful in understanding structural and spectroscopic phenomena. For example, the tug-of-war between hybridization and hyperconjugation was used to rationalize the peculiar properties of blue-shifting H-bonds (also referred to as "improper" H-bonds). These supramolecular interactions display the reversal of the usual red-shift behavior of H-bonds in the seemingly paradoxical C–H bond shortening and the blue-shift in the respective IR stretching frequency.[44] This behavior reflects the importance of rehybridization as a structural force controlling X–H bond length in the process of $X{-}H\cdots Y$ bond formation (Fig. 15.23).[45]

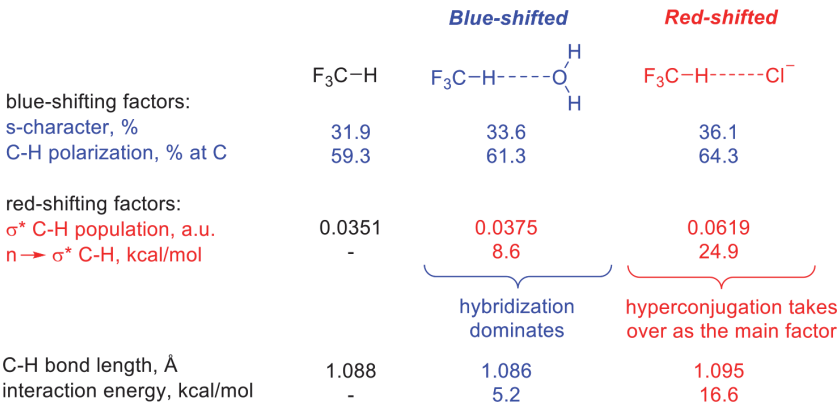

Figure 15.23. Structures, energies, and NBO analysis of blue- and red-shifted H-bonds at the MP2/6–31+G* level of theory.

Source: From Ref. [35].

The delicate balance of charge transfer and rehybridization becomes apparent when examining the H-bonds between F_3C–H and water (blue-shifted) and F_3C–H and Cl^- (red-shifted, Fig. 15.23).[35] Relative to the "free" C–H bond, the C–H-bonds in the two complexes show an increase in s-character, C–H bond polarization, and σ^*_{C-H} population. Interestingly, the F_3C–H$\cdots Cl^-$ H-bond actually shows a greater percentage of s-character (36.1% vs. 33.6%) and a more polarized bond (64.3% vs. 61.3%), relative to the blue-shifted F_3C–H$\cdots OH_2$ H-bond. Despite these larger changes in hybridization and polarization, the hyperconjugative charge transfer acts as a dominating force leading to the red-shifted F_3C–H$\cdots Cl^-$ H-bond. Interestingly, at greater F_3C–H$\cdots Cl^-$ separations, the C–H bond initially undergoes a contraction (that should lead to a blue-shift in the respective IR stretching frequency) and only at the distances where the direct orbital overlap with the chloride lone pair is sufficiently strong to make the $n_{Cl} \rightarrow \sigma^*_{C-H}$ interaction to be sufficiently strong, the C–H bond contraction is replaced by C–H bond elongation. This analysis illustrates that the same factors are involved in the two H-bond types and it is the balance of them that controls the observed shift in the C–H stretching frequency.

To further illustrate the generality of hybridization/hyperconjugation competition, let us discuss the relative strength of C–H bonds in halogen-substituted methanes (Fig. 15.24). These simple molecules display surprisingly rich structural reorganization patterns, depending on the type and number of halogen atoms.

If only vicinal stereoelectronic interactions are considered, one would expect that the C–H bond in fluoromethane would be longer than the C–H bond of methane due to the contribution of $n_F \rightarrow \sigma^*_{C-H}$ interaction. Indeed, such elongation is observed (1.089 vs. 1.091 Å) along with the red-shift of the respective IR-stretching C–H frequency (2992 vs. 2976 cm^{-1}). However, this simple explanation stops working when the second fluorine is introduced or when fluorine is changed to a heavier halogen. In both cases, the C–H bond gets shorter and a blue-shift is observed for the C–H stretching frequencies.

What can explain the red-shift of these frequencies in fluoroalkanes when compared to methane? Furthermore, how can one explain

molecule	ν(CH)[a]	C-H (Å)[b]	C-H hybridization[b]
CH_4	**2992**	1.0892	$sp^{3.00}$
FCH_3	2976	1.0906	$sp^{2.76}$
F_2CH_2	2984	1.0901	$sp^{2.53}$
F_3CH	2990	1.0885	$sp^{2.27}$
$ClCH_3$	3012	1.0862	$sp^{2.76}$
Cl_2CH_2	3025	1.0841	$sp^{2.61}$
Cl_3CH	3034	1.0829	$sp^{2.51}$
$BrCH_3$	3027	1.0852	$sp^{2.70}$
Br_2CH_2	3040	1.0832	$sp^{2.52}$
Br_3CH	3050	1.0815	$sp^{2.42}$

[b]: calculated at M06-2X/6-311++G(d,p)

(a)

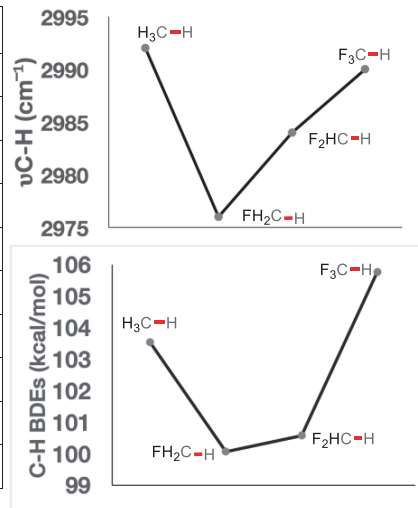

(b)

Figure 15.24. (a) C–H frequencies, lengths, and hybridizations for methane and a series of mono-, di- and tri-substituted halomethanes. (b) Trends for C–H bond BDEs and stretching frequencies for methane and its fluoro-substituted analogues.

the fact that trend is just the *opposite* for chloro- and bromoalkanes? This is a case where a detailed analysis of the interplay of the stereoelectronic effects and hybridization is crucial and only the power of computational analysis can provide an answer.

Below are presented the experimental IR C–H frequencies alongside C–H bond lengths and hybridizations for methane and its halo-substituted analogues. In parallel, we show the trends in C–H BDEs. Note that the energies follow the same general trend as the respective ν(C–H) values: decreasing at first and progressively increasing the further fluorine atoms are added. The unusual behavior is unique for fluorine. For the other halogens, progressive blue-shift in the C–H stretching frequency and bond contraction are observed.

A closer analysis of NBO data illustrates how substituting hydrogen for fluorine causes a series of perturbations in the other three C–H bonds (Fig. 15.25). First, due to Bent's rule,[46] carbon has to put more *p*-character into the C–F bond. Because the overall *p*-character is conserved (i.e., there are only 3 p-AOs), the C–H bonds at the same atom have to rehybridize (from sp^3 to $sp^{2.76}$, according to NBO analysis). The increase in *s*-character is expected to make this C–H bond shorter. Thus, the observed elongation relative to the C–H bonds of methane is even more impressive, suggesting the dominating structural effect of hyperconjugative $n_F \rightarrow \sigma^*_{C-H}$ interactions. Indeed,

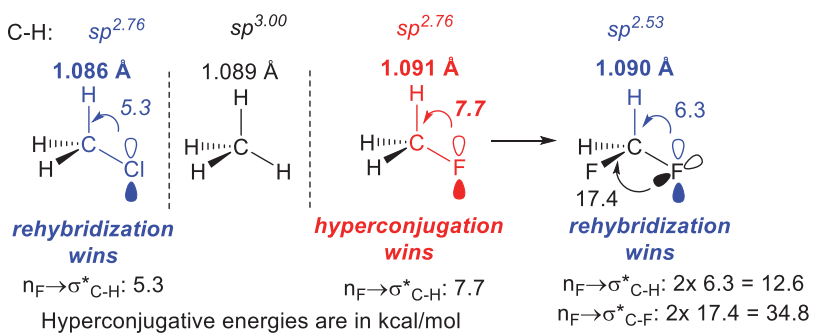

Figure 15.25. Tug-of-war between (re)hybridization and hyperconjugation. Hyperconjugative interactions are given in kcal/mol.

NBO analysis suggests that these are quite strong — worth up to 7.7 kcal/mol. In this case, hyperconjugation wins over hybridization, leading to C–H bond elongation and weakening. The structural effects are fully consistent with the energetic and spectroscopic effects: i.e., decrease in the C–H BDE and red-shift in the IR stretching frequency.

On the other hand, chloromethane follows what is expected based on Bent's rule: the C–H bond is shortened and it shows by being blue-shifted in the IR spectra when compared to methane. This is a case where rehybridization overcomes hyperconjugation. NBO analysis clearly shows that hyperconjugation is 2.4 kcal/mol weaker in comparison to fluoromethane: the energy of $n_{Cl} \rightarrow \sigma^*_{C-H}$ interaction is 5.3 kcal/mol. This decrease is due to the greater length of the C–Cl bond which diminishes the π-type $n_{Cl} \rightarrow \sigma^*_{C-H}$ vicinal overlap. Because the $\sim sp^{2.76}$ hybridization of C–H bonds in fluoro- and chloromethane is almost identical (but different from methane!), the weaker hyperconjugation in chloromethane allows the rehybridization effect to manifest itself fully (chlorine's lone pairs are not as good donors as fluorine's), in making the C–H bond shorter and stronger.

Further replacement of H atoms by fluorines increases the frequency of the C–H stretch, a sign that the bond is getting stronger and shorter. Indeed, the expected bond shortening is reproduced in the calculated structures. This trend is consistent with rehybridization imposed by Bent's rule. For example, carbon uses $sp^{2.27}$ hybrid in the C–F bonds of CHF_3. Furthermore, the additional F atoms introduce another stereoelectronic effect into the picture: the lone pairs can interact with the much stronger σ^*_{C-F} acceptors (i.e., a manifestation of the general anomeric effect). The competition between hyperconjugation ($n_F \rightarrow \sigma^*_{C-H}$) and the anomeric effect ($n_F \rightarrow \sigma^*_{C-F}$) combined with further increase on the *s*-character in the C–H bond (rehybridization) bring the stretching frequency for this bond close to that for the C–H bonds of methane.

15.9 Marcus analysis

In this section, we will introduce Marcus theory as a tool for detecting stereoelectronic stabilization of TS structures and show how it was used to identify a new effect that facilitates radical fragmentations (Fig. 15.26). After a sequence of reactions that convert aromatic enynes into α-Sn-substituted naphthalenes into a six-membered cyclic radical, the penultimate species of the overall cascade, the final step involves a C–C bond scission. The efficiency of fragmentation can be enhanced by stabilizing the rational design of radical leaving groups (Fig. 15.26).[47] The stabilization, conveniently evaluated by the equation given in Fig. 15.27, illustrates that the presence of a lone pair adjacent to the radical center stabilizes the radical.

However, fragmentation leading to the formation of the *more* stable α-oxy radical ($\bullet CH_2OMe$) was calculated to be *less* exergonic that the analogous fragmentation that forms the propyl radical. The paradoxical lower thermodynamic driving force for the formation of a *more* stable O-containing radical can be explained by the presence of a selective reactant stabilization. A through-bond (TB) interaction

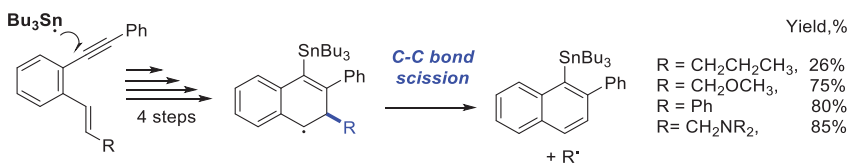

Figure 15.26. Efficiency of fragmentation can be increased by proper substitution at the alkene terminus.

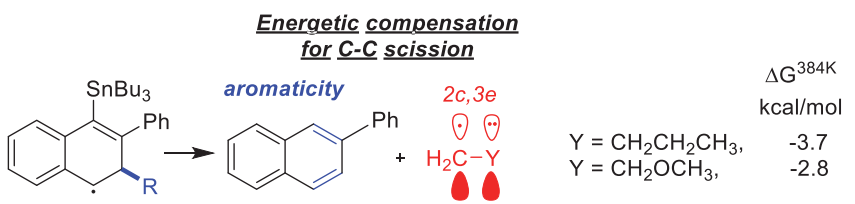

Figure 15.27. Two ways to compensate a C–C scission: aromaticity and the radical stabilizing 2*c*,3*e* interaction.

between the benzylic radical and the lone pair at the δ-position was suggested as the source of this reactant stabilization.[47]

Such TB coupling between two nonbonding orbitals populated with three electrons (the lone pair of X and the radical center) can rationalize the calculated fragmentation exergonicities by providing additional stabilization to the benzylic radical with a β-X group. From a practical point of view, such stabilization should deactivate the reactant and make this fragmentation less efficient. However, in another seeming paradox, the experimental data clearly suggest the opposite — the fragmentations were clearly assisted by the presence of a lone pair next to the radical center of the departing species.

These observations can only be resolved if the presence of oxygen leads to selective TS stabilization that exceeds such stabilization of the reactant. It was suggested that the odd-electron TB communication between the radical and the lone pair through the σ-bridge is increased at the TS and, thus, can serve as the source of additional TS stabilization. NBO analysis of orbital interactions supported this hypothesis.[47] However, the quantitative accuracy of NBO dissections (based on localized dominant Lewis structures as a starting point) suffers in TS structures due to their intrinsically delocalized nature and, thus, an alternative way of evaluating the energetics of TS structures can be useful.

Of course, direct comparison of barrier heights for different reactions is the most straightforward way for making such evaluations. However, for reactions with different exothermicity, such comparison is complicated by thermodynamic contributions to the barrier (the consequence of the increased stability of reaction products). In order to distinguish such contribution from the direct stabilizing effects intrinsic to the TS structure, one can turn to Marcus theory.[48,49]

Marcus theory dissects activation energy into two contributions: the intrinsic energy barrier height and the thermodynamic contribution (Eq. (15.2)).

$$\Delta E^{\ddagger} = \Delta E_0^{\ddagger} + \frac{1}{2}\Delta E_{rxn} + \Delta E_{rxn}^2/16\Delta E_0^{\ddagger} \qquad (15.2)$$

Stereoelectronic differences in the TS can be identified by examining the intrinsic barrier $\Delta E_0^{\ddagger}$, i.e., the barrier of a thermoneutral process lacking the thermodynamic contributions. The intrinsic barrier can be estimated from the rearranged Eq. (15.3) if both the activation and reaction energies are known

$$\Delta E_0^{\ddagger} = \frac{\Delta E^{\ddagger} - \frac{1}{2}\Delta E_{rxn} + \sqrt{(\Delta E^{\ddagger})^2 - \Delta E^{\ddagger}\Delta E_{rxn}}}{2} \qquad (15.3)$$

To eliminate the complication associated with the difference in the entropic penalties, one can focus on reaction energies ΔE (rather than free energies, ΔG). When thermodynamic contributions to the barrier are removed, significant differences in the TS energies still remain (1–2 kcal/mol for X = CH_2OR and *ca.* 6 kcal/mol for X = CH_2NMe_2). These large effects on the fragmentation barrier originate from electronic communication between the nonbonding orbitals, which weakens the bridging σ-bond in the TS.

The increase in TB interaction through stretched bonds is documented by NBO orbital interaction energies. In the fragmentation process, the energy of the σ^*-antibonding bridge orbital is lowered, decreasing the ΔE_{ij} term for the stabilizing interaction that couples the nonbonding orbitals (i.e., the radical and lone pair). In addition, as the fragmentation progresses, the $\sim sp^3$ σ-bond is transformed into two p-orbitals (one π-bonded in naphthalene and the other in a $2c$–$3e$ "half-bond"), increasing overlap between interacting orbitals. Together these interactions are responsible for selective TS stabilization for the fragmentation process.

An analysis of the Marcus theory shows that intrinsic reaction barriers for the fragmentation are decreased by the presence of heteroatoms with lone pairs. This finding illustrates the utility of Marcus dissection for finding and evaluating selective TS stabilization effects. It does not identify what the interaction may be. Other theoretical methods such as MO and NBO analyses suggested that such stereoelectronic effect is the TB interaction described above. This interaction serves as a stereoelectronic conduit for the observed acceleration of the bond scission.

In summary, one can apply the Marcus theory to analyze stereoelectronic effects in TS structures with the following sequence of steps:

(1) Calculate the activation barrier $\Delta E^{\ddagger}$ and the reaction energy of the process, ΔE_{rxn}.
(2) Use the $\Delta E^{\ddagger}$ and ΔE_{rxn} values to calculate Marcus intrinsic barriers $\Delta E_0^{\ddagger}$ using Eq. (15.3).
(3) Because $\Delta E_0^{\ddagger}$ values are free from thermodynamic and entropic contributions, they reflect the electronic component of reactivity. Comparison of intrinsic barriers for different substituents allows the detection of the stereoelectronic effects in the TSs.
(4) This approach can be complemented with NBO analysis of reactants, TSs, and products to gauge the relative importance of individual interactions and evaluate their evolution along the reaction path.

The caveat in using such Marcus analysis is that the bonds broken and formed in reactions should be similar. For two bonds of drastically different nature with different shapes of potential energy surfaces, the accuracy of simple Marcus description of such surfaces as two parabolas may become inadequate. For example, the use of Marcus theory for comparison cycloaddition to alkenes vs. alkynes is expected to suffer from a systematic error associated with the different intrinsic strengths of π-bonds in these two functionalities.[50,51]

15.10 Distortion analysis — Interaction energies

Another useful method for detecting stereoelectronic effects is distortion analysis (see Chapter 13).[52] Distortion analysis dissects the activation barrier for cycloadditions (or other bimolecular reactions) into distortion and interaction energies. Distortion describes the energy penalty for adopting the TS geometry by the reactants, whereas interaction energy reflects energy lowering due to covalent and noncovalent interaction between the reactants in the TS geometry. Here we will only summarize the key points needed for the application of this approach toward stereoelectronic analysis.

The Distortion–Interaction model is based on the dissection of the activation barrier, $\Delta E^{\ddagger}$, in two components:

(1) The energy to distort reactants to the geometry they adopt in the TS, ΔE_{dist}. This can be interpreted as the ***penalty*** the reactants have to pay to adopt the TS geometry $\Delta E_{\text{dist}} > 0$.
(2) The interaction energy, ΔE_{int}, that ***lowers*** the overall energy due to covalent and noncovalent interactions during the TS $\Delta E_{\text{int}} < 0$.

For bimolecular reactions, stereoelectronic effects that lead to TS stabilization are often manifested via an increase of stabilizing interaction energy between the fragments. Such effects can be detected as considerable deviations in the correlation of distortion energy with full activation barriers. The activation barrier $\Delta^{E\ddagger}$ can be calculated as:

$$\Delta E^{\ddagger} = \Delta E_{\text{dist}} + \Delta E_{\text{int}} \tag{15.4}$$

In summary, one can apply the Distortion–Interaction model to analyze stereoelectronic effects in TS structures with the following methodology for bimolecular processes (i.e., cycloadditions):

(1) One needs to calculate the geometries of reactants and TS using an appropriate theoretical method.
(2) One calculates the energy of each reactant separately in their TS specific geometries with two single-point calculations (one for each distorted reactant).
(3) ΔE_{dist} is calculated by subtracting the energy of the two fragments of the TS by the energy of the separated reactants in the ground state:

$$\Delta E_{\text{dist}} = \Delta E_{\text{reactants}}^{\text{TSgeometry}} - \Delta E_{\text{reactants}}^{\text{GSgeometry}} \tag{15.5}$$

For example, one can lower the activation barrier of a system by destabilizing one of the reactants, therefore paying less distortion penalties.

(4) Now one can simply calculate ΔE_{int} by the following difference: $\Delta E_{\text{int}} = \Delta E^{\ddagger} - \Delta E_{\text{dist}}$.
(5) Since ΔE_{int} directly reflects the electronic interactions in the TS, the impact of different stereoelectronic effects can be evaluated by this term. A straightforward approach is to vary different substituents in both reactants and see how that changes the activation barrier. Then one can compare how much of those variations come from stereoelectronics and design solutions for a particular problem.

As an example, let us illustrate how distortion analysis can be used to identify specific orbital stabilizing effects in the TS of the noncatalyzed alkyne–azide cycloaddition (Fig. 15.28).[53]

Figure 15.28(a) illustrates that activation energy increases linearly with the amount of total distortion energy require to "bend" the alkyne to its geometry in the TS. Increased strain activates the alkyne by forcing it to a geometry that is closer to the one it would have during the TS. In other words, the alkyne can "pre-pay" the distortion penalty to reach the TS geometry. However, the simple

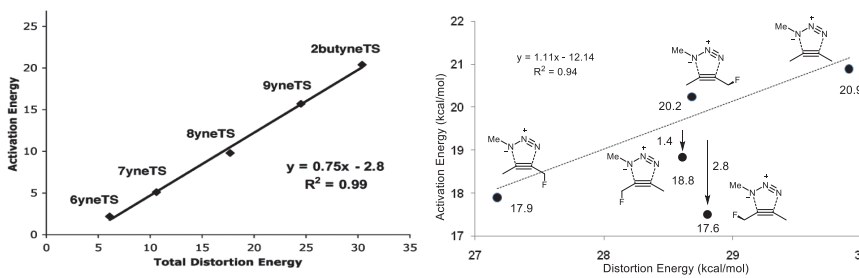

(a) (b)

Figure 15.28. (a) Correlation between activation and distortion energies of (cyclo)alkynes in cycloaddition reactions. Energies in kcal/mol. (b) Correlation between activation and distortion energies of (α-fluorosubstitued)-2-butynes in cycloaddition reactions. Deviations from the straight line indicate additional stabilizing interactions in the TS. (Calculations at the B3LYP/6-31G(d) level.)

Source: Reprinted with permission from Refs. [53a, 54], respectively.

correlations of distortion and activation energies become more complicated when stereoelectronic effects are present.

As an example, let us analyze Fig. 15.28(b), where the same cycloaddition reaction shows different behavior. It is clear that data for several substrates with a σ-acceptor at the propargylic carbon do not follow the linear correlation. Two points deviate from the linear trend most significantly, with activation energies much smaller than expected from the respective distortion energies. This behavior is evidence of stereoelectronic effects that stabilize the TS. We will discuss the specific nature of these effects later in this section.

When viewed through the prism of the distortion analysis, these strategies for TS stabilization can be quantified (Table 15.1) as increases in "interaction energy." Increase in this interaction relative to the isolated alkyne is mostly due to an increase in the population of donor π^* orbital which is empty in the reactant but gains some electronic density in the TS.[53] Because the above interaction is manifested to a greater degree in the TS, this effect fits the classic definition of TS stabilization — the ideal scenario for selective reaction acceleration.

However, the utility of distortion analysis does not stop here. Table 15.1 also illustrates the decrease in the "distortion energy" of the alkyne component for the fluoro-substituted substrates. So, which stereoelectronic effects are manifested in the increased interaction energy and in the decreased distortion penalty?[53a]

15.10.1 *Stereoelectronic origin of decrease in distortion energies*

The formation of both 1,4- and 1,5-isomers of the triazole product is facilitated via hyperconjugative assistance to alkyne bending and C$\cdots$N bond formation provided by antiperiplanar σ-acceptors at the propargylic carbons, diminishing the distortion energy. As the alkyne is bent, the in-plane π-bond becomes a better donor, therefore making hyperconjugative interactions with the appropriately positioned substituents stronger. This reinforcement is illustrated by the symmetric bending of 2-butyne relative to fluoro-2-butyne (Fig. 15.29), with a decreasing energy cost of bending in the following

Table 15.1. Activation, reaction, distortion, and interaction energies for 2-butyne and 1-fluoro-2-butyne TSs at the B3LYP/6-31G(d) level of theory.

	Distortion energy-alkyne (kcal/mol)	Distortion energy-azide (kcal/mol)	Distortion energy total (kcal/mol)	Interaction energy, kcal/mol)	Activation energy (kcal/mol)	Reaction energy (kcal/mol)
2-butyne	10.12	19.78	29.90	−9.01	20.89	−67.8
Gas phase	10.11	20.14	30.26	−7.66	22.62	−70.4
CPCM (H_2O)[a,b]						
1,5-*app* Gas	9.25	19.41	28.66	−9.83	18.83	−69.8
phase	9.50	19.75	29.25	−8.41	20.84	−71.2
CPCM (H_2O)[a,b]						
1,5-*gauche*	10.23	18.52	28.75	−11.20	17.55	−69.8
Gas phase	10.10	18.57	28.67	−8.52	20.15	−71.2
CPCM (H_2O)[a,b]						
1,4-*app* Gas	8.74	18.43	27.17	−9.27	17.90	−70.8
phase	8.93	18.75	27.68	−7.77	19.91	−72.3
CPCM (H_2O)[a,b]						
1,4-*gauche*	10.16	18.52	28.68	−8.44	20.24	−70.8
Gas phase	10.06	18.85	28.91	−7.71	21.20	−72.3
CPCM (H_2O)[a,b]						

Notes: [a]B3LYP/6-31G(d) geometry.
[b]Radii = UA0.

order: 2-butyne > 1-fluoro-2-butyne (gauche) > 1-fluoro-2-butyne (synperiplanar) > 1-fluoro-2-butyne (antiperiplanar).

15.10.2 *Stereoelectronic origin of increase in interaction energies*

The above stabilizing effect increases even further in the full TS, where the azide is close to the bent alkyne. In the TS, the propargylic

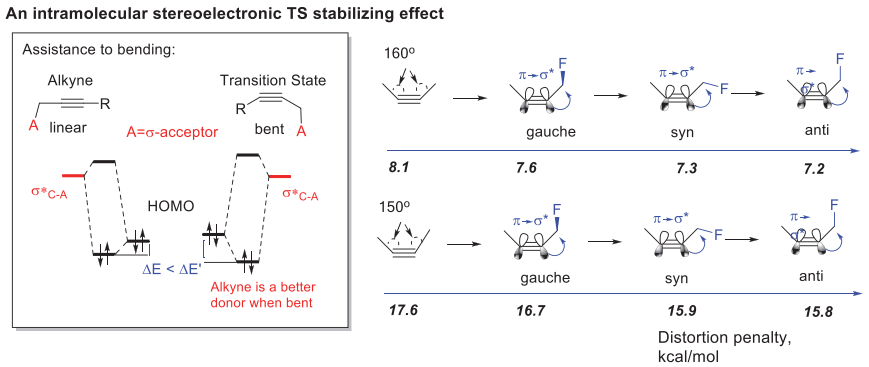

Figure 15.29. (a) Stereoelectronic basis for assistance to alkyne bending utilized in TS stabilization in azide-alkyne cycloadditions. (b) Symmetric bending scan of butyne and 2-fluorobutyne in the gauche, synperiplanar, and antiperiplanar conformations.

acceptor facilitates bond formation (Fig. 15.30) due to the interaction of a strategically placed antiperiplanar C–F bond with the reacting π-system, σ^*_{C-F}. The donor ability of the distorted "incipient" bond (i.e., the "hyperconjugative assistance to bond formation"[54]) decreases the activation energy by 1.4 kcal/mol. NBO analysis suggests that π^* of the alkyne (i.e., its LUMO) becomes populated as the azide approaches. The high-energy π^*-orbital is usually empty, but in the cycloaddition TS, it has sufficient electron density (transferred from the azide in the bond forming interaction) to serve as a very strong donor. Figure 15.30 illustrates that orbital mixing in the TS leads to larger stabilization when delocalization into a propargylic acceptor ($\pi + \pi^* \rightarrow \sigma^*_{CF}$) is conceivable. This qualitative analysis is fully supported by NBO dissection of the individual stereoelectronic contributions.

In the other case, where an even greater barrier lowering is observed in Fig. 15.29 (~2.8 kcal/mol), fluorine plays a different stereoelectronic role: a 1,5-gauche fluoro substituent can interact with the C–H bond of the methyl azide moiety via a stabilizing Me···F interaction that can be considered as a weak C−H···X hydrogen bond with a considerable electrostatic component.

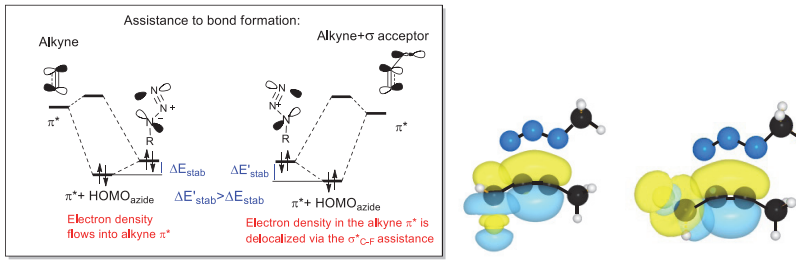

Figure 15.30. (a) Electronic basis for TS stabilization. The increase in the alkyne π^* population due to the C$\cdots$N bond-forming interaction complements the effect of propargylic acceptor on alkyne bending. (b) NBO plots for orbital interactions between the propargylic σ-acceptors and the reacting in-plane alkyne π-bond in the cycloadditions TS for the antiperiplanar (left) and gauche (right) orbital arrangements.

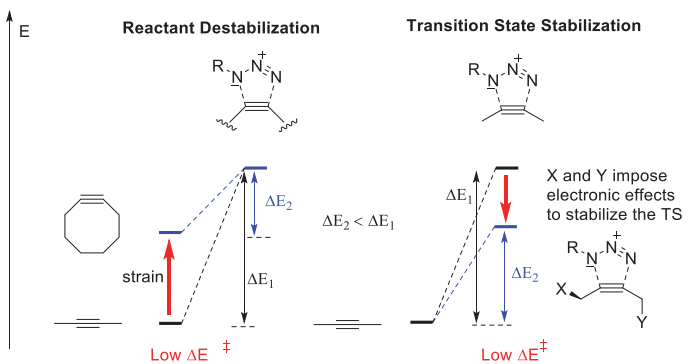

Figure 15.31. Comparison of alternative strategies for acceleration of copper-free click reactions.

Comparison of reactant destabilization by strain and TS stabilization by stereoelectronic effects suggest two complementary strategies toward faster noncatalyzed click cycloadditions (Fig. 15.31).

Combined with strain activation, the stereoelectronic strategy can incorporate several components. As a result, one can design a system that exploits both distortion and stereoelectronic effects for interaction in the TS. The combination of several strategies was estimated to provide greater than 10,000-fold acceleration, upon the

transition from the regular cyclooctyne to its electronically activated derivatives.[53b]

15.11 Conclusions and practical considerations

We have described several computational approaches for the detection and quantification of stereoelectronic orbital interactions using computational methods: from conformational analysis to thermochemistry, from wavefunction dissections to global energy components revealed by distortion analysis and Marcus theory. We hope that with the help of these quantitative techniques, the large variety of stereoelectronic effects suggested in the literature can be critically evaluated, bringing a new level of computational rigor in this field.

References

1. (a) Deslongchamps, P. (1984). *Stereoelectronic Effects in Organic Chemistry* (Pergamon Press, Oxford); (b) Kirby, A. J. (1983). *The Anomeric Effect and Related Stereoelectronic Effects at Oxygen* (Springer-Verlag, Berlin, New York).
2. Alabugin, I. V. and Manoharan, M. (2004). Effect of double hyperconjugation on the apparent donor ability of σ-bonds: Insights from the relative stability of δ-substituted cyclohexyl cations, *J. Org. Chem.*, 69, pp. 9011–9024.
3. Kirby, A. J. (1996). *Stereoelectronic Effects* (Oxford University Press, Oxford).
4. For definitions see: Wheeler, S. E., Houk, K. N., Schleyer, P. v. R. and Allen, W. D. (2009). A hierarchy of homodesmotic reactions for thermochemistry, *J. Am. Chem. Soc.*, 131, pp. 2547–2560.
5. (a) Hehre, W. J., Ditchfield, R., Radom, L. and Pople, J. A. (1970). Molecular orbital theory of the electronic structure of organic compounds. V. Molecular theory of bond separation, *J. Am. Chem. Soc.*, 92, pp. 4796–4801; (b) Radom, L., Hehre, W. J. and Pople, J. A. (1971). Molecular orbital theory of the electronic structure of organic compounds. VII. Systematic study of energies, conformations, and bond interactions, *J. Am. Chem. Soc.*, 93, pp. 289–300; (c) Hehre, W. J., Radom, L., Schleyer, P. v. R. and Pople, J. A. (1986). *Ab Initio Molecular Orbital Theory* (Wiley-Interscience, New York).
6. Hoffmann, R. (1971). Interaction of orbitals through space and through bonds, *Acc. Chem. Res.*, 4, pp. 1–9.
7. Mohamed, R. K., Peterson, P. W. and Alabugin, I. V. (2013). Concerted reactions that produce diradicals and zwitterions: Electronic, steric, conformational, and kinetic control of cycloaromatization processes, *Chem. Rev.*, 113, pp. 7089–7129.

8. (a) Schottelius, M. J. and Chen, P. (1996). 9,10-Dehydroanthracene: *p*-Benzyne-type biradicals abstract hydrogen unusually slowly, *J. Am. Chem. Soc.*, 118, pp. 4896–4903; (b) Pickard, F. C. IV, Shepherd, R. L., Gillis, A. E., Dunn, M. E., Feldgus, S., Kirschner, K. N., Shields, G. C., Manoharan, M. and Alabugin, I. V. (2006). Ortho effect in the Bergman cyclization: Electronic and steric effects in hydrogen abstraction by 1-substituted naphthalene 5,8-diradicals, *J. Phys. Chem. A*, 110, pp. 2517–2526.
9. Bender, D. M., Peterson, J. A., McCarthy, J. R., Gunaydin, H., Takano, Y. and Houk, K. N. (2008). Cyclopropanecarboxylic acid esters as potential prodrugs with enhanced hydrolytic stability, *Org. Lett.*, 10, pp. 509–511.
10. Rogers, D. W., Matsunaga, N., Zavitsas, A. A., McLafferty, F. J. and Liebman, J. F. (2003). The conjugation stabilization of 1,3-butadiyne is zero, *Org. Lett.*, 5, pp. 2373–2375.
11. Jarowski, P. D., Wodrich, M. D., Wannere, C. S., Schleyer, P. V. R. and Houk, K. N. (2004). How large is the conjugative stabilization of diynes? *J. Am. Chem. Soc.*, 126(46), pp. 15036–15037.
12. Alabugin, I. V., Gilmore, K. and Peterson, P. (2011). Hyperconjugation, *WIREs Comput. Mol. Sci.*, 1, pp. 109–141.
13. (a) Bickelhaupt, F. M. and Baerends, E. J. (2003). The case for steric repulsion causing the staggered conformation of ethane, *Angew. Chem. Int. Ed.*, 42, pp. 4183–4188; See also: (b) Cappel, D., Tullmann, S., Krapp, A. and Frenking, G. (2005). Direct estimate of the conjugative and hyperconjugative stabilization in diynes, dienes, and related compounds, *Angew. Chem. Int. Ed.*, 44, pp. 3617–3620; (c) Fernandez, I. and Frenking, G. (2007). Direct estimate of conjugation and aromaticity in cyclic compounds with the EDA method, *Faraday Discuss.*, 135, pp. 403–421; (d) Fernandez, I. and Frenking, G. (2006). Direct estimate of the strength of conjugation and hyperconjugation by the energy decomposition analysis method, *Chem. Eur. J.*, 12, pp. 3617–3629.
14. (a) Mo, Y., Wu, W., Song, L., Lin, M., Zhang, Q. and Gao, J. (2004). The magnitude of hyperconjugation in ethane: A perspective from *ab initio* valence bond theory, *Angew. Chem. Int. Ed.*, 43, pp. 1986–1990; (b) Mo, Y. and Gao, J. (2007). Theoretical analysis of the rotational barrier of ethane, *Acc. Chem. Res.*, 40, pp. 113–119.
15. Weinhold, F. and Carpenter, J. E. (1988). Some remarks on non-orthogonal orbitals in quantum chemistry, *J. Mol. Struct. (THEOCHEM)*, 165, pp. 189–202.
16. Corcoran, C. T. and Weinhold, F. (1980). Antisymmetrization effects in bond-orbital models of internal rotation barriers, *J. Chem. Phys.*, 72, pp. 2866–2868.
17. (a) Weinhold, F. (2001). Chemistry: A new twist on molecular shape, *Nature*, 411, pp. 539–540; (b) Weinhold, F. (2003). Rebuttal to the Bickelhaupt-Baerends case for steric repulsion causing the staggered conformation of ethane, *Angew. Chem. Int. Ed.*, 42, pp. 4188–4194.

18. Gross, K. C. and Seybold, P. G. (2001). Substituent effects on the physical properties and pKa of phenol, *Int. J. Quantum Chem.*, 85, pp. 569–579.
19. Weinhold, F. and Schleyer, P. v. R. (1998). *Encyclopedia of Computational Chemistry* (Wiley, New York), p. 3, 1792.
20. Reed, A. E. and Weinhold, F. (1985). Natural localized molecular-orbitals, *J. Chem. Phys.*, 83, pp. 1736–1740.
21. Reed, A. E., Curtiss, L. A. and Weinhold, F. (1988). Intermolecular interactions from a natural bond orbital, donor–acceptor viewpoint, *Chem. Rev.*, 88, pp. 899–926.
22. Alabugin, I. V. and Zeidan, T. A. (2002). Stereoelectronic effects and general trends in hyperconjugative acceptor ability of s bonds, *J. Am. Chem. Soc.*, 124, pp. 3175–3185.
23. (a) Badenhoop, J. K. and Weinhold, F. (1997). Natural bond orbital analysis of steric interactions, *J. Chem. Phys.*, 107, pp. 5406–5422; (b) Badenhoop, J. K. and Weinhold, F. (1999). Natural steric analysis of internal rotation barriers, *Int. J. Quantum Chem.*, 72, pp. 269–280.
24. Weisskopf, V. F. (1975). Of atoms, mountains, and stars: A study in qualitative physics, *Science*, 187, pp. 605–612.
25. Foster, J. M. and Boys, S. F. (1960). Canonical configurational interaction procedure, *Rev. Mod. Phys.*, 32, pp. 300–302.
26. Edmiston, C. and Ruedenberg, K. (1963). Localized atomic and molecular orbitals, *Rev. Mod. Phys.*, 35, pp. 457–465.
27. Pipek, J. and Mezey, P. G. (1989). A fast intrinsic localization procedure applicable for *ab initio* and semiempirical linear combination of atomic orbital wave functions, *J. Chem. Phys.*, 90, pp. 4916–4926.
28. Zubarev, D. Y. and Boldyrev, A. I. (2008). Developing paradigms of chemical bonding: Adaptive natural density partitioning, *Phys. Chem. Chem. Phys.*, 10, pp. 5207–5217.
29. (a) Bickelhaupt, F. M., Baerends, E. J. and Evert, J. (2000). Kohn-Sham density functional theory: Predicting and understanding chemistry, *Rev. Comput. Chem.*, 15, pp. 1–86; (b) te Velde, G., Bickelhaupt, F. M., Baerends, E. J., Van Gisbergen, S. J. A., Snijders, J. G. and Ziegler, T. (2001). Chemistry with ADF, *J. Comp. Chem.*, 22, pp. 931–967; See also (c) Ziegler, T. and Rauk, A. (1977). On the calculation of bonding energies by the Hartree Fock Slater method. I. The transition state method, *Theo. Chim. Acta*, 46, pp. 1–10; (d) Morokuma, K. (1971). Molecular orbital studies of hydrogen bonds III. C=O...H-O hydrogen bond in $H_2CO...H_2O$ and $H_2CO...2H_2O$, *J. Chem. Phys.*, 55, pp. 1236–1244.
30. Fernandez, I. and Frenking, G. (2007). Direct estimate of the conjugative and hyperconjugative stabilization in diynes, dienes, and related compounds, *Faraday Discuss.*, 135, pp. 403–421.
31. Mo, Y. (2006). Intramolecular electron transfer: Computational study based on the orbital deletion procedure (ODP), *Curr. Org. Chem.*, 10, pp. 779–790.
32. (a) Mo, Y. and Peyerimhoff, S. D. (1998). Theoretical analysis of electronic delocalization, *J. Chem. Phys.*, 109, pp. 1687–1697; (b) Mo, Y., Zhang, Y. and

Gao, J. (1999). A simple electrostatic model for trisilylamine: Theoretical examinations of the n $\rightarrow$ σ^* negative hyperconjugation, pπ $\rightarrow$ dπ bonding, and stereoelectronic interaction, *J. Am. Chem. Soc.*, 121, pp. 5737–5742; (c) Mo, Y., Gao, J. and Peyerimhoff, S. D. (2000). Energy decomposition analysis of intermolecular interactions using a block-localized wave function approach, *J. Chem. Phys.*, 112, pp. 5530–5538; (d) Mo, Y., Subramanian, G., Ferguson, D. M. and Gao, J. (2002). Cation-π interactions: An energy decomposition analysis and its implication in δ-opioid receptor-ligand binding, *J. Am. Chem. Soc.*, 124, pp. 4832–4837; (e) Mo, Y., Song, L., Wu, W. and Zhang, Q. (2004). Charge transfer in the electron donor–acceptor complex BH_3NH_3, *J. Am. Chem. Soc.*, 126, pp. 3974–3982; (f) Mo, Y. and Gao, J. (2000). An *ab initio* molecular orbital-valence bond (MOVB) method for simulating chemical reactions in solution, *J. Phys. Chem.*, 104, pp. 3012–3020; (g) Mo, Y. and Gao, J. (2000). *Ab initio* QM/MM simulations with a molecular orbital-valence bond (MOVB) method: Application to an SN2 reaction in water, *J. Comp. Chem.*, 21, pp. 1458–1469; (h) Mo, Y. (2004). Resonance effect in the allyl cation and anion: A revisit, *J. Org. Chem.*, 69, pp. 5563–5567.

33. Mo, Y. (2010). Computational evidence that hyperconjugative interactions are not responsible for the anomeric effect, *Nat. Chem.*, 2, pp. 666–671.
34. Fulton, R. L. (1993). Sharing of electrons in molecules, *J. Phys. Chem.*, 97, pp. 7516–7529.
35. (a) Coulson, C. A. (1939). The electronic structure of some polyenes and aromatic molecules. VII. bonds of fractional order by the molecular orbital method, *Proc. R. Soc. A*, 158, pp. 413–428; (b) Wiberg, K. B. (1968). Application of the Pople-Santry-Segal CNDO method to the cyclopropylcarbinyl and cyclobutyl cation and to bicyclobutane, *Tetrahedron*, 24, pp. 1083–1096; (c) Mayer, I. (1983). Charge, bond order and valence in the *ab initio* SCF theory, *Chem. Phys. Lett.*, pp. 270–274.
36. Bader, R. F. W. (1990). *Atoms in Molecules: A Quantum Theory* (Oxford University Press, Oxford).
37. (a) Becke, A. D. and Edgecombe, K. E. (1990). A simple measure of electron localization in atomic and molecular systems, *J. Chem. Phys.*, 92, pp. 5397–5403; (b) Silvi, B. and Savin, A. (1994). Classification of chemical bonds based on topological analysis of electron localization functions, *Nature*, 371, pp. 683–686.
38. For a more detailed analysis of saturated heterocycles, see Alabugin, I. V. (2000). Stereoelectronic interactions in cyclohexane, 1,3-dioxane, 1,3-oxathiane, and 1,3-dithiane: W-effect, $\sigma_{C-X} \leftrightarrow \sigma^*_{C-H}$ interactions, anomeric effect — what is really important? *J. Org. Chem.*, 65, pp. 3910–3919.
39. Gomes, G. P., Vil', V., Terent'ev, A. and Alabugin, I. V. (2015). Stereoelectronic source of the anomalous stability of bis-peroxides, *Chem. Sci.*, 6, pp. 6783–6791.
40. For a similar analysis, see Rzepa, H. The conformation of acetaldehyde: A simple molecule, a complex explanation? http://doi.org/10.15200/winn.142795.56009.

41. (a) Guirgis, G. A., Drew, B. R., Gounev, T. K. and Durig, J. R. (1998). Conformational stability and vibrational assignment of propanal, *Spectrochim. Acta Mol. Biomol.*, 54, pp. 123–143; (b) Karabastos, G. J. and Hsi, N. (1965). Structural studies by nuclear magnetic resonance. X. conformations of aliphatic aldehydes, *J. Am. Chem. Soc.*, 87, pp. 2864–2870.
42. (a) Jalbouta, A. F., Basso, E. A., Pontes, R. M. and Das, D. (2004). Hyperconjugative interactions in vinylic systems: The problem of the barrier to methyl rotation in acetone, *THEOCHEM*, 677, pp. 167–171; (b) Allinger, N. L., Hirsch, J. A., Miller, M. A. and Tyminski, I. J. (1969). Conformational analysis. LXV. Calculation by the Westheimer method of the structures and energies of a variety of organic molecules containing nitrogen, oxygen, and halogen, *J. Am. Chem. Soc.*, 91, pp. 337–343.
43. Blanksby, S. J. and Ellison, G. B. (2003). Bond dissociation energies of organic molecules, *Acc. Chem. Res.*, 36, pp. 255–263.
44. (a) Hobza, P. and Havlas, Z. (2000). Blue-shifting hydrogen bonds, *Chem. Rev.*, 100, pp. 4253–4264; (b) Budesinsky, M., Fiedler, P. and Arnold, Z. (1989). Triformylmethane: An efficient preparation, some derivatives, and spectra, *Synthesis*, 1989, pp. 858–86; (c) Boldeskul, I. E., Tsymbal, I. F., Ryltsev, E. V., Latajka, Z. and Barnes, A. J. (1997). Reversal of the usual v(C-H/D) spectral shift of haloforms in some hydrogen-bonded complexes, *J. Mol. Struc.*, 436, pp. 167–171; (d) Hobza, P., Spirko, V., Selzle, H. L. and Schlag, E. W. (1998). Anti-hydrogen bond in the benzene dimer and other carbon proton donor complexes, *J. Phys. Chem. A*, 102, pp. 2501–2504.
45. Alabugin, I. V., Manoharan, M., Peabody, S. and Weinhold, F. (2003). Electronic basis of improper hydrogen bonding: A subtle balance of hyperconjugation and rehybridization, *J. Am. Chem. Soc.*, 125, pp. 5973–5987.
46. For a more detailed review on orbital hybridization, see: Alabugin, I. V., Bresch, S. and dos Passos Gomes, G. (2014). Orbital hybridization: A key electronic factor in control of structure and reactivity, *J. Phys. Org. Chem.*, 28(2), pp. 147–162. See also: Alabugin, I. V., Bresch, S. and Manoharan, M. (2014). Hybridization trends for main group elements and expanding the Bent's rule beyond carbon: More than electronegativity, *J. Phys. Chem.*, 118, pp. 3663–3677.
47. (a) Mondal, S., Gold, B., Mohamed, R. K. and Alabugin, I. V. (2014). Design of leaving groups in radical C–C fragmentations: Through-bond 2c–3e interactions in self-terminating radical cascades, *Chem. Eur. J.*, 20(28), pp. 8664–8669; (b) Mohamed, R. K., Mondal, S., Gold, B., Evoniuk, C. J., Banerjee, T., Hanson, K. and Alabugin, I. V. (2015). Alkenes as alkyne equivalents in radical cascades terminated by fragmentations: Overcoming stereoelectronic restrictions on ring expansions for the preparation of expanded polyaromatics, *J. Am. Chem. Soc.*, 137(19), pp. 6335–6349.
48. (a) Marcus, R. A. (1956). On the theory of oxidation-reduction reactions involving electron transfer. I. *The J. Chem. Phys.*, 24(5), pp. 966–978; (b) Marcus, R. A. (1964). Chemical and electrochemical electron-transfer

theory, *Annu. Rev. Phys. Chem.*, 15(1), pp. 155–196; (c) Marcus, R. A. (1968). Theoretical relations among rate constants, barriers, and Broensted slopes of chemical reactions, *J. Phys. Chem.*, 72(3), pp. 891–899. For alternative models, see also: (d) Evans, M. G., Polanyi, M. (1938). Inertia and driving force of chemical reactions. *Trans. Faraday Soc.*, 34, pp. 11–24; (e) Koeppl, G. W., Kresge, A. J. (1973). Marcus rate theory and the relationship between Brønsted exponents and energy of reaction, *J. Chem. Soc., Chem. Comm.*, 11, pp. 371–373.

49. For the application of Marcus theory to radical reactions, see: (a) Alabugin, I. V. and Manoharan, M. (2005). 5-endo-dig radical cyclizations: "The poor cousins" of the radical cyclizations family, *J. Am. Chem. Soc.*, 127(26), pp. 9534–9545. For potential caveats, see: (b) Osuna, S. and Houk, K. N. (2009). Cycloaddition reactions of butadiene and 1,3-dipoles to curved arenes, fullerenes, and nanotubes: Theoretical evaluation of the role of distortion energies on activation barriers, *Chem. Eur. J.*, 15(47), pp. 13219–13231.
50. Alabugin, I. V. and Gold, B. (2013). "Two functional groups in one package": Using both alkyne π-bonds in cascade transformations, *J. Org. Chem.*, 78, pp. 7777–7784.
51. Osuna, S. and Houk, K. N. (2009). Cycloaddition reactions of butadiene and 1,3-dipoles to curved arenes, fullerenes, and nanotubes: Theoretical evaluation of the role of distortion energies on activation barriers, *Chem. Eur. J.*, 15, pp. 13219–13231.
52. (a) Ess, D. H. and Houk, K. N. (2007). Distortion/interaction energy control of 1,3-dipolar cycloaddition reactivity, *J. Am. Chem. Soc.*, 129, pp. 10646–10647. For examples in cycloadditions: (b) Ess, D. H., Jones, G. O. and Houk, K. N. (2008). Transition states of strain-promoted metal-free click chemistry: 1,3-dipolar cycloadditions of phenyl azide and cyclooctynes, *Org. Lett.*, 10, pp. 1633–1636; (c) Schoenebeck, F., Ess, D. H., Jones, G. O. and Houk, K. N. (2009). Reactivity and regioselectivity in 1,3-dipolar cycloadditions of azides to strained alkynes and alkenes: A computational study, *J. Am. Chem. Soc.*, 131, pp. 8121–8133.
53. (a) Gold, B., Shevchenko, N., Bonus, N., Dudley, G. B. and Alabugin, I. V. (2012). Selective transition state stabilization via hyperconjugative and conjugative assistance: Stereoelectronic concept for copper-free click chemistry, *J. Org. Chem.*, 77, pp. 75–89; (b) Gold, B., Dudley, G. B. and Alabugin, I. V. (2013). Moderating strain without sacrificing reactivity: Design of fast and tunable noncatalyzed alkyne–azide cycloadditions via stereoelectronically controlled transition state stabilization, *J. Am. Chem. Soc.*, 135, pp. 1558–1569.
54. Schoenebeck, F., Ess, D. H., Jones, G. O. and Houk, K. N. (2009). Reactivity and regioselectivity in 1,3-dipolar cycloadditions of azides to strained alkynes and alkenes: A computational study, *J. Am. Chem. Soc.*, 131(23), pp. 8121–8133.